Ultrafast Ultrasound Imaging in Pediatric and Adult Cardiology Techniques, Applications, and Perspectives

Olivier Villemain, Jérôme Baranger, Mark K. Friedberg, Clément Papadacci, Alexandre Dizeux, Emmanuel Messas, Mickael Tanter, Mathieu Pernot, Luc Mertens

Ultrafast Ultrasound Imaging in Pediatric and Adult Cardiology: Techniques, Applications and Perspectives

Olivier Villemain, MD, PhD[1,2]; Jérôme Baranger, MS[1]; Mark K. Friedberg, MD[2]; Clément Papadacci, PhD[1]; Alexandre Dizeux, PhD[1]; Emmanuel Messas, MD, PhD[3]; Mickael Tanter, PhD[1]; Mathieu Pernot, PhD[1#] / Luc Mertens, MD, PhD[2#]

[1]Physics for Medicine Paris, Inserm, ESPCI Paris, CNRS, PSL University, Paris, France
[2]Labatt Family Heart Centre, The Hospital for Sick Children, University of Toronto, Toronto, Ontario, Canada.
[3]Centre de Référence des Maladies Vasculaires Rares, Hôpital Européen Georges-Pompidou, Assistance Publique - Hôpitaux de Paris (APHP), Paris, France.

[#]Mathieu Pernot and Luc Mertens contributed equally to this work, and are joint senior authors.

Corresponding Author:
Olivier Villemain, MD, PhD
Labatt Family Heart Centre, The Hospital for Sick Children, University of Toronto, Toronto, Ontario, Canada.
Physics for Medicine Paris, Inserm, ESPCI Paris, CNRS, PSL University, Paris, France
Telephone: (1) 416-813-7654. Fax: (1) 416-813-5857
E-mail : olivier.villemain@sickkids.ca

COMPETING INTERESTS: No

FUNDING: No

ABSTRACT

Ultrasound techniques currently used in echocardiography are limited by conventional frame rates. Ultrafast ultrasound imaging is able to capture images at frame rates up to 100 times faster compared to conventional imaging. Specific applications of this technology have been developed and tested for clinical use in pediatric and adult cardiac imaging. These include ultrafast Doppler or vector flow imaging, shear wave imaging, electromechanical wave imaging and backscatter tensor imaging. The principles of these applications are explained in the manuscript with illustrations on how these methods could be applied in clinical practice. Ultrafast ultrasound has great clinical potential in the assessment of cardiac function, in noninvasive hemodynamic analysis, while providing novel techniques for imaging coronary perfusion and evaluating rhythm disorders.

Key Words: ultrafast imaging • echocardiography • pediatric • cardiac function • shunt • valvulopathy

ABBREVIATIONS:
BTI: backscatter tensor imaging
CHD: congenital heart disease
CUDA: coronary ultrafast Doppler angiography
EDPVR: end-diastolic pressure-volume relationship
ESPVR: end-systolic pressure-volume relationship
ETI: elastic tensor imaging
MS: myocardial stiffness
SWE: shear wave elastography
VFI: vector flow imaging

KEY POINTS

- Ultrafast ultrasound imaging could be a central non-invasive imaging tool, particularly in congenital and pediatric cardiology.

- Myocardial stiffness (MS) assessment by ultrafast ultrasound imaging has the potential to become a cornerstone of ultrasound imaging in cardiology, particularly for the noninvasive assessment of systolic and diastolic physiology.

- Further clinical developments could potentially reduce the need for cardiac MRI or imaging techniques requiring radiation.

Echocardiography plays a central role in the diagnosis and management of patients in cardiology. During the last two decades, new technologies based on conventional ultrasound have been introduced in clinical practice and have improved diagnostic capabilities[1]. Tissue Doppler imaging[2], strain imaging[3], and 3D echocardiography[4] have found a role in clinical cardiology in most centers. While most of these techniques have been widely accepted in adult cardiology, application of these techniques in children is limited by specific technical challenges[5]. The heart rates in newborns is three times higher than in the adults requiring higher temporal resolution, while the anatomical structures are much smaller requiring higher spatial resolution. Moreover, in patients with congenital heart disease (CHD) the morphology and loading conditions can be highly variable. This result in the need for specific ultrasound tools for pediatric and congenital heart disease. In addition, the noninvasive assessment of cardiac function remains a major challenge in cardiology, especially in adults. Systolic and diastolic function require a specific evaluation and new parameters independent of loading conditions.

Most of the current tools in echocardiography rely on focused ultrasound beams which intrinsically limits frame rate and temporal resolution. Ultrafast ultrasound imaging was recently introduced based on utilizing of non-focused plane wave ultrasound technology. This results in very high temporal resolution compared to conventional imaging[6]. The challenge is spatial resolution for which different solutions have been developed, such as the use of multiple plane waves for one image (coherent compounding) or the use of harmonic frequencies[7]. Applications of ultrafast imaging include novel methods to assess myocardial viscoelastic properties (such as myocardial stiffness)[8,9], imaging of coronary flow[10], intracavitary blood flow[11,12,13], as well as tools to study electromechanical coupling[14,15], and methods to study the dynamic characteristics of myocardial fiber orientation[16,17,18]. Ultrafast

ultrasound has also been proposed for noninvasive central venous pressure assessment[19,20,21] and brain perfusion[22].

The introduction of ultrafast ultrasound created a revolution in non-invasive diagnostic capabilities but, at the moment, is only at the clinical proof-of-concept stage. Further clinical developments could potentially reduce the need for cardiac MRI or imaging techniques requiring radiation[23]. Therefore, the objective of this review is to provide an overview of ultrafast ultrasound imaging in cardiology.

ULTRAFAST ULTRASOUND IMAGING

Basic concepts

Although the use of ultrasonic plane-wave transmission rather than line-per-line focused beam transmission has been long researched, clinical application of this technology was only recently made possible through increasing computing capabilities and the introduction of powerful graphical processing unit (GPU)-based platforms, making it possible the appearance of ultrasound system capable of acquiring per channel data in real-time does[6]. Ultrafast imaging is based on the use of plane or divergent waves, instead of focused beams (figure 1). Plane and divergent waves are generated by applying a plane or circular delay on the elements of the transducer. In both cases, it is possible to reconstruct an entire image with a single emission. This imaging approach results in a lower spatial resolution and a lower contrast of the images. A technique that can be used to overcome this limitation is to use multiples plane waves transmitted at slightly different angles to obtain one image. Indeed, coherent combination of compounded plane-wave transmissions (also called coherent plane wave compounding) allows to recover high-spatial resolution without compromising the high

frame rate[24]. Consequently, blood and tissue motion in addition to tissue structure may now be explored using high frame rate ultrasound imaging (Central figure).

Blood flow

- *Ultrafast Doppler imaging*

Conventionally, blood flow is detected with Doppler ultrasound by discriminating signals according to their temporal characteristics based on Doppler frequency[25]. As red blood cells tend to move faster than the surrounding tissue, their Doppler frequency is generally higher and the two signals can be separated by applying a temporal filter. In cardiac imaging, myocardial tissue also moves which can make blood flow detection more challenging. In ultrafast ultrasound, all the pixels (or voxels) in a frame (or in a volume) are analyzed simultaneously, and both the temporal and spatial characteristics of the incoming signals can be exploited[26]. Tissue is known to be more spatially coherent than blood and is far less deformable than blood. This results in the signals from neighboring pixels or voxels inside a tissue area to be more likely correlated to one another. This additional spatial information allows the use of spatiotemporal filters which dramatically improve blood detection[27]. Hence, ultrafast ultrasound not only brings the possibility of imaging high velocity flow but also the ability to efficiently discriminate blood flow from tissue movement.

- *Coronary ultrafast Doppler angiography (CUDA)*

Flow detection in the coronary circulation requires distinguishing the blood signal from myocardial movement. This becomes even more challenging for imaging the coronary microvasculature (with a diameter less than 100 micrometer). The use of specific and adaptive spatiotemporal filters[28] allows separation of blood flow from tissue motion resulting in the evaluation of coronary anatomy, intramural perfusion and coronary flow reserve. It has recently been shown that the spatiotemporal information using transthoracic ultrafast

ultrasound allows the detection of coronary flow in epicardial and intramyocardial arteries in both children and adults[10]. Furthermore, power Doppler imaging may be used to quantify blood volume. It relies on the measurement of pulse-to-pulse decorrelation of returning echocardiographic signals from the same location to detect moving objects.

- *Ultrafast vector flow imaging (VFI)*

Doppler imaging as implemented in clinical scanners is often limited to the measurement of blood flow velocities in the axial direction, i.e. detecting blood moving toward or away from the probe. Detecting more complex flow velocities in different directions is made possible by vector flow imaging (VFI). Initially this was based on speckle tracking of injected microbubbles using contrast echocardiography (echo-PIV or echographic particle image velocimetry)[29]. This method was developed using conventional imaging techniques at lower frame rates thereby having an intrinsic frame rate limitation. For application in children, the use of contrast agents is limiting the clinical applicability. VFI can also be achieved without contrast agents by tracking blood speckles. This approach is generally referred to as blood speckle flow imaging[30] and requires temporal high-pass filtering to remove the high-amplitude signals from surrounding tissues. The advantage of vector flow imaging is its low angle dependence, which differentiates it from spectral Doppler techniques., It allows visualizing and estimating the direction and velocities of blood flow in different directions from any angle. While 2D velocities estimations are limited by through-plane motion, ideally three or four-dimensional techniques could overcome this problem. The main technical limitation is the huge amount of information gathered by 4D flow acquisitions making implementation on standard scanners impossible[31]. Velocity information in different directions allows for analysis of the exact vector velocity[32]. This gives access to more complex flow patterns including visualization of intracardiac or intravascular vortices[33].

Vortex imaging has been demonstrated to provide important novel hemodynamic information contributing to novel insights in cardiovascular pathophysiology and disease detection[34].

Tissue motion – Imaging of Natural Waves and Shear Wave Elastography

Higher frame rates make it possible to visualize short-lived myocardial tissue motion that cannot be detected by conventional ultrasound techniques. This allows the detection of myocardial mechanical waves that occur naturally (for instance at the time of valve closure or following electrical depolarization) or are generated by transmitting an external mechanical wave by acoustic radiation force.

- *Electromechanical wave imaging*

Electromechanical coupling is a very short-lived cardiac event and is the time between electrical and mechanical activation[35]. This delay is very short, in the order of tens of milliseconds[36] and propagation of the electromechanical activity throughout the myocardium occurs at a similar delay. At the tissue level, the depolarization of myocardial regions triggers electromechanical activation (i.e., the first time at which the muscle transitions from a relaxation to a contraction state). Spatially, this electromechanical activation forms the electromechanical wave (EW) front that follows the propagation pattern of the electrical activation sequence. At high frame rate, EWI uses radio frequency (RF)-based cross-correlation, a motion estimation method that can be up to ten times more accurate than brightness mode (B mode)-based speckle tracking. Ultimately, being able to see the motion (displacement or deformation) induced by the electromechanical coupling makes it possible to deduce the mechanical activation timing and to map it[37,38].

- *Assessment of myocardial stiffness - Natural waves and Shear Wave Elastography (acoustic radiation force)*

What is Stiffness ?

Stiffness is an intrinsic property of soft tissues which reflects the tissue composition and organization at macroscopic and microscopic scales. Conventional assessment of soft tissue elastic properties (i.e stiffness) relies on mechanical testing, for instance by the application of an external stress and the measurement of the resulting tissue deformation. This general principle was developed for the analysis of elastic properties of ex vivo tissues, and was then applied to noninvasive imaging techniques such as ultrasound or MRI through the quantification of the deformation using the so-called static elastography technique. Static elastography, however, do not provide quantitative estimate of tissue stiffness because the stress distribution cannot be quantified accurately in vivo, even though strain imaging provides accurate deformation estimates. Dynamic and transient elastography techniques[39,40] based on the propagation of low frequency shear waves in tissue were introduced to overcome this limitation. These approaches relying tracking shear wave propagation at ultrafast frame rates (>1000fps) in order to quantify the shear velocity are quantitative thanks to the direct link between shear velocity and shear modulus [see Equation 1]. They have now been implemented in commercial medical devices and ultrasound scanners to quantify stiffness in the breast, in the liver or in skeletal muscles.

Assuming that the medium is incompressible, infinite and isotropic, shear wave propagation velocity can be derived from general equations of the dynamic theory of linear elasticity[41]. Therefore, the stiffness of a tissue can be approximated by estimating the shear modulus (μ) using the equation relating shear wave speed (Vc), shear modulus (μ) and local density (ρ, knowing that ρ is almost constant in soft tissue ($\rho \approx 1000$ kg/m^3):

$$Vc = \sqrt{\frac{\mu}{\rho}} \qquad \text{Equation [1]}$$

The shear modulus is one of several quantities used to measure the stiffness of tissue or a material. Ultrafast imaging measured Vc in soft tissue is in the order of 1-10 meter per second, or 1-10 millimeter per millisecond which is within the temporal resolution of ultrafast

imaging. A shear wave can be generated by using an external force or can occur naturally related to intrinsic mechanical events such as valve closure.

External stimulus – Acoustic radiation force (figure 2)

External generation of shear waves in soft tissue is possible using acoustic radiation force[42,43]. A short burst of several hundred microseconds (µs) of focused ultrasound can induce micrometric tissue displacements in a small zone of myocardium (figure 2). The transient mechanical excitation produces a shear wave in the low kHz frequency range which propagates through the myocardium at a velocity that is dependent on the tissue stiffness[44]. Using ultrafast imaging, myocardial wall motion is subtracted from the average wall motion during the acquisition, resulting in net tissue motion induced by the shear wave. Shear wave speed (Vc) can be computed at each depth of the image using the spatiotemporal data of the shear wave propagation. Finally, the shear modulus µ (i.e., stiffness) can be derived at each location using the equation described above [1].

The advantage of using an external stimulus to generate the shear waves is that it is possible to choose both the timing of the tissue assessment and the location of the shear wave source. Indeed, as the shear wave is generated by an external stimulus controlled by the investigator, one can estimate MS at any time during the cardiac cycle[45]. As MS varies throughout the cardiac cycle[45,46], one may analyze the MS at a time in the cardiac cycle relevant to the clinical question (during the active relaxation or the diastasis for example). The disadvantage of this approach is that it is only possible to analyze a specific myocardial region, as defined by the push area. Indeed, because of the physical properties of both the shear wave (kHz frequency) and the medium (e.g. thickness of the myocardium), shear wave propagation is interpretable only in an area of few centimeters[47]. It is therefore a segmental analysis and only reflects MS within the interrogated area.

Measuring shear wave velocities using Internal events (figure 3)

The motion of the heart can be summarized as contraction and relaxation of the myocardium. However, the local motion of cardiovascular tissues over the course of an entire cardiac cycle results from various transient events such as the valvar closing and opening, sudden changes in blood pressure and electrical conduction through the myocardium. All these events elicit natural mechanical waves during the cardiac cycle[14]. During valve closure, a transient mechanical shear wave is generated at the annulus of the valve which propagates through the adjacent myocardium[48]. Similarly, sudden changes in chamber pressure, such as following atrial contraction, generates LV myocardial stretch that propagates from base to apex with a speed proportional to myocardial elasticity[49]. The correlation between MS and myocardial stretch, using the theory of wave propagation in elastic tubes (Moens-Korteweg equation), deserves further exploration[50,51].

Currently, only shear waves induced by the aortic or mitral valve closure have been used to deduce the shear velocity. The advantage of this approach is that only ultrafast imaging, without external acoustic radiation force is used to visualize and analyze natural phenomena[52]. Usually, tissue velocity is estimated between every two frames using a Doppler autocorrelation method. Anatomical acceleration M-mode maps are extracted along the midline of the LV septum, yielding a spatiotemporal representation of the local tissue acceleration throughout the cardiac cycle[52]. Moreover, the amplitude of these natural waves is at least one order of magnitude higher than acoustic radiation force induced shear waves and thus are more easily visualized[47]. The main disadvantage of this approach is that the timing is dictated by the intrinsic event, i.e. the shear waves are visible just after atrioventricular valve closure (during isovolumetric contraction) and just after the semilunar valve closure (during isovolumetric relaxation). Finally, such low frequency natural shear waves present large wavelengths and their velocity may be affected by the geometry of the myocardial wall making the link between shear velocity and stiffness more complicated[53] (figure 4).

Technical limitations

For relatively isotropic and homogeneous organs, such as the liver or breast, the Young's modulus can be derived directly from the shear velocity ($E \approx 3\mu$). However, the propagation of elastic waves in the myocardium is more complex due to the active properties of the muscle fibers. This includes stiffness changing over time, the anisotropy of the tissue relating to the complex fiber orientation of different layers, and the geometry of the ventricles[54]. These parameters induce a complex wave propagation in three dimensions, complicating the relationship between shear wave characteristics and elastic tissue properties[55].

Moreover, guided wave propagation occurs when the wall thickness and the shear wavelength become on the same order of magnitude[56]. The main consequence of this is a modification of the shear wave velocity and therefore, an alteration of the link between Vc and μ [Equation 1]. Correia et al, using Shear Wave Imaging (external stimulus) showed, that the accuracy could be significantly altered for myocardial stiffness superior to 25 KPa and for myocardial wall thickness inferior to 5-mm, in vitro on calibrated mimicking tissue phantoms using a phased-array probe (2.75MHz)[57].

The reader should keep in mind that the link between shear velocity and stiffness is not always straightforward. Therefore, shear velocity should be always reported by researchers. Complex biomechanical modelling can be used in order to derive viscoelastic parameters such as the elastic anisotropic properties of the myocardium[58].

Tissue structure – Myocardial Fiber Imaging

Availability of a technique for assessing myocardial fiber orientation would have important potential clinical applications in patients with CHD. First myocardial fiber orientation can be altered in patients with CHD and this can be important for understanding myocardial mechanics. Secondly myocardial fiber disarray can occur during ventricular remodeling

resulting in myocardial regional dysfunction. Two different techniques based on ultrafast scanning allow to imaging of fiber orientation.

- *Backscatter Tensor Imaging (BTI)*

BTI is based on ultrafast ultrasound acquisitions which are used to quantify the spatial coherence of ultrasonic speckle echoes at each point of the plane[59] or the volume[16,60]. Spatial coherence allows us to understand the tissue structure and reveals the anisotropy of the ultrasonic speckle in the myocardium (see figure 9 for example). The BTI technique is also able to provide information on each fiber size and each fiber structure[61].

- *Elastic tensor imaging (ETI)*

Elastic tensor imaging (ETI) is based on shear wave imaging[17]. Shear wave propagate faster in the direction of the fibers. By using several SWE acquisitions along different directions, fiber orientation can be estimated compared to histology as gold standard[17]. This technique was initially based on the rotation of a 2D ultrasound probe to create shear waves propagating along different directions. More recently, 3D elastic tensor imaging (3D-ETI) was introduced[18].

APPLICATIONS IN PEDIATRIC AND CONGENITAL CARDIOLOGY

From a very practical point of view, the variation of frame rate (from conventional to ultrafast) does not change the clinical constraints of pediatric cardiology. Indeed, the transmission/reception frequency, allowing to optimize the spatial resolution and thus to adapt to the anatomy explored, will be generally the same whatever the frame rate. In addition, the type of probe (phased-array or linear) and angular dependency remains the same. In the future, the manufacturer (and not the practitioner) will need to adapt their

systems and their "probe to system" transmissions in order to allow the application of ultrafast imaging in pediatrics (as in adult cardiology).

For this reason, little precision will be given in this "Applications" chapter on the type of equipment, type of probe or emission/reception frequencies, as these parameters will be broadly comparable to daily clinical practice. In the case of an exception (e.g. for CUDA only demonstrated with a linear probe for technical reasons), precision will be provided.

In this chapter, the applications will therefore be grouped by type of disease and not by age group (traditionally used in pediatrics) because all the techniques presented do not have specific limits according to the patient's age or weight.

Diastolic function

Analysis of diastolic function is a major challenge in pediatric and congenital cardiology. Parameters conventionally used in adult cardiology, such as pulsed-wave Doppler (PW), continuous-wave Doppler (CW) or tissue Doppler imaging (TDI), have limitations in pediatrics for two main reasons: (1) these parameters are highly dependent on heart rate, heart size and body size; (2) the variable anatomy and loading conditions in children. Dragulescu et al. have shown that conventional ultrasound seems inadequate in pediatric patients with cardiomyopathy to assess diastolic dysfunction[62]. More generally, the use of parameters depending on anatomy are limited in the presence of cardiac malformations[63,64]. Ultrafast ultrasound allows a direct measurement of viscoelastic properties and diastolic MS. Initial data are promising. Using myocardial shear wave imaging, Song et al showed that measuring diastolic stiffness was feasible in children and they published reference values in healthy controls[65]. Villemain et al showed that SWE could differentiate healthy volunteers and patients with sarcomeric hypertrophic cardiomyopathy[8] (figure 5). It is interesting to note that the degree of diastolic dysfunction using conventional methods (echo and MRI parameters)

correlated with MS assessment. More validation is required but shear wave echocardiography is a promising new tool for the assessment of diastolic function in children. Nevertheless, whether by SWE or natural shear waves, the assessment of MS currently remains segmented (limited to one specific myocardial segment). This is the main application limitation of these techniques at the moment.

Ultrafast ultrasound-based flow imaging techniques could also be used for studying diastolic function. The more detailed 2D/3D flow information as obtained with vector flow imaging, could be used to calculate energy losses during diastole and to calculate intraventricular pressure gradients during early filling representing early diastolic suction. Initial studies in adults have been promising but clinical validation in children is still required[66].

Shunt and valvar disease

The hemodynamic assessment of shunts and valvulopathies is complex in pediatric cardiology. Doppler-based imaging techniques are currently used in clinical settings using spectral analysis techniques (CW and PW Doppler) for local velocities and color-coded techniques (CFI) for flows in a wider field of view. Unfortunately, these techniques have inherent limitations including angle dependence and low frame rates, which may lead to inaccurate evaluation[67]. In addition, both CFI and PW Doppler are limited by aliasing limiting the velocity range and leading to potentially ambiguous results. Currently, estimation of valvar regurgitation is at best semi-quantitative. Clearly, improved flow measurements are necessary.

Ultrafast VFI possesses important advantages. Due to its low dependency of insonation angle and its temporal resolution, it can more accurately estimate flow and pressure gradients[13]. Accordingly, it may be well-suited to study the hemodynamic consequences of a valvulopathy and for estimating flows through shunts, for example atrial septal defects

(ASD) and ventricular septal defects (VSD) (figure 6)[68]. Recently, Hansen et al compared VFI to conventional Doppler imaging showing that VFI may provide additional information – in particular the flow analysis at the apex or in the ascending aorta – compared to conventional echocardiography and become an useful additional diagnostic tool[69]. Fadnes et al also showed that complex intraventricular flow velocity patterns could be quantified using ultrafast VFI by comparing VFI with color flow imaging and pulsed wave Doppler using manual angle correction [68]. The angle independence of this parameter could significantly decrease variability when measuring peak velocities in shunt flows. In addition, more recently, the same group demonstrated the feasibility of VFI for cardiac 4D acquisitions (figure 7)[33]. They compared their results to MRI and showed that 4D VFI is reliable and robust. Using this approach, it might be possible to analyze and assess, in a volumetric acquisition and at the bedside, all relevant hemodynamic parameters (e.g. flow, pressure, size) of shunts and in different valvulopathies. One of the challenges for this approach remains the very large datasets that have to be stored and processed. While feasibility has been proven, it will take a long journey to a readily available clinical application.

Coronary imaging

Coronary ultrafast Doppler angiography (CUDA, figure 8) allows unprecedented noninvasive visualization and analysis of intramural coronary perfusion and hemodynamics such as coronary flow reserve. Osmanski et al showed that it is technically possible to visualize the coronary flow (veins and arteries)[26]. Then, Maresca et al, on an animal model (using a coronary flow probe as gold standard) and on the human in transthoracic (children and adults), proved that the CUDA allowed an anatomical and hemodynamic analysis of the coronary flow[10]. No other imaging tool is currently able to assess hemodynamic flow variation in the coronaries. Using power-velocity integrals (PVI), a metric proportional to

flow rate[70], CUDA could provide a quantitative measurement of coronary flow variations and coronary flow reserve. This direct measurement of flow variation overcomes the limitations of existing Doppler techniques allowing for the analysis of dynamic myocardial perfusion. Nevertheless, except this clinical publication, to our knowledge there are no other published clinical applications of CUDA. In addition, a linear probe was used in this work, which theoretically limits clinical applications in cardiology. It will therefore be necessary to provide evidence of the application of this technique with a phased-array probe. Notwithstanding, a variety of pathological situations could benefit from this new capability. For example, right ventricular (RV) function is a major determinant of prognosis in pulmonary arterial hypertension (PAH). RV hypertrophy (RVH) triggered by pressure overload is initially compensatory but often leads to RV failure. Despite similar RV afterload and mass, some patients develop adaptive RVH (concentric with retained RV function), while others develop maladaptive RVH, characterized by dilatation, fibrosis, and RV failure[71]. The differentiation of adaptive versus maladaptive RVH is imprecise, but adaptive RVH is associated with better functional capacity and survival. Although RV ischemia is implicated in contributing to RV dysfunction in PAH, the (mal)adaptive myocardial perfusion response to this situation is currently largely unexplored because of a lack of available tools. CUDA could help us to understand and differentiate between adaptive versus maladaptive responses. Likewise, functionally univentricular hearts, have unique, but largely unexplored aberrations in myocardial perfusion. Files and Arya recently suggested that, while the hypertrophied RV in PAH frequently shows an inadequate microvascular density and subsequent ischemia, ischemia is uncommon in hypoplastic left heart syndrome (HLHS)[72]. One hypothesis for systemic RV dysfunction is a mismatch between myocardial perfusion and tissue restructuring (fibrosis, collagen deposition)[73]. An intramural coronary imaging tool would likely advance our understanding and analysis of the pathophysiological mechanisms. For

example, in unoperated patients with congenitally corrected transposition of the great arteries, Hauser et al. showed using positron emission tomography (PET) that systemic RV coronary reserve is decreased in the absence of ischemic symptoms[74]. Thus, the global impairment of stress flow dynamics may indicate altered global vasoreactivity, and quantitative changes in microcirculation suggest that their role in the pathogenesis of systemic RV dysfunction is important. Nevertheless, PET is difficult to use in clinical practice, especially in pediatrics[75]. Access to a non-invasive bedside tool such as CUDA to analyze myocardial perfusion could be revolutionary. Lastly, Nield et al investigated whether specific coronary Doppler patterns intra-operatively predicted adverse early myocardial events[76] in newborns with transposition of the great arteries (TGA) before the arterial switch operation (ASO). Forty patients were recruited and thirty-two had intra-operative transesophageal echo (TEE) plus an epicardial echo during surgery. They showed that flow reversal in the left coronary artery was associated with the composite endpoint (post-operative ST changes, ventricular tachycardia, need for extracorporeal membrane oxygenation) and for delayed chest closure. This suggest that in TGA, myocardial perfusion analysis just before and immediately after ASO provides information relevant to the patient's clinical course. Further clinical studies using ultrafast imaging are expected to explore intramural perfusion in these patients.

Cardiomyopathies and myocardial fibers' structure

Risk assessment in a variety of pediatric cardiomyopathies using conventional imaging parameters is quite limited[62]. The ultrafast ultrasound tools previously described could aid in the evaluation and risk-stratification of pediatric cardiomyopathies and myocarditis. In adults[77] and in children[8], Villemain et al explored the potential of SWE to distinguish normal from pathological, finding a strong correlation between SWE and clinical status. In addition, they showed, using ETI (previously compared to histology[17]), that the fractional anisotropy

was different between healthy volunteers and patients with sarcomeric hypertrophic cardiomyopathy (figure 5). Therefore, ultrafast imaging could shed new light on myocardial function and structure, especially in a variety of cardiomyopathies. In a systematic review on hypertrophic cardiomyopathies published in 2002, Barry J. Maron[78] noted that the "LV myocardial architecture is disorganized […] with multiples intercellular connections often arranged on chaotic alignment and with expanded interstitial (matrix) collagen,". This is supported by previous work that tried to link myocardial histological explorations and MS[79]. The degree and type of myocardial fibers' disarray are different according to the etiology of cardiomyopathy, and the new tools presented (shear wave imaging, BTI, ETI) allow a quantitative assessment of this disarray. Despite this, shear wave imaging and ETI currently only allow for segmental exploration which could limit the use of these techniques for the global understanding of a myocardial fiber's disarray.

Moreover, due to frame rate limitations, myocardial (or ventricular) structure cannot yet be observed in the beating heart, with the exception of BTI (figure 9)[16]. The understanding of cardiac embryogenesis is a fundamental point in the analysis of the function and structure in CHD. For example, the RV has distinct embryological origins from the second heart field, whereas the LV originates from first heart field progenitors[80]. This may partially explain the varied molecular response and histological makeup of the RV relative to the LV when subjected to increased pressure and volume loading, and may explain why well-proven medical therapies for LV dysfunction fail to show benefit for RV failure[81]. The normal RV myocardial architecture has superficial circumferential fibers and deep longitudinal fibers with the majority of contraction occurring longitudinally from base to apex under normal circumstances. Ultimately, BTI could alter our comprehension of the link between myocardial structure and cardiac function, especially in CHD where abnormal myocardial structure may determine function, however this remains vastly under-explored.

Rhythm disorders

Ultrafast ultrasound allows to study electromechanical coupling which could be useful for the detection of abnormal electrical activation patterns. Recently, by studying fifteen pediatric patients with Wolff-Parkinson-White syndrome, Melki et al[38] have shown that electromechanical wave imaging (EWI) was capable of consistently localizing accessory pathways with better accuracy than traditional clinical tools such as Arruda's or Boersma's one (figure 10) using invasive electrophysiology as the gold standard. Studying electrical activation patterns may facilitate preparation of complex electrophysiology procedures and may help in better understanding pathophysiology of bundle branch block. At the present time, the main limitation of the EWI lies in its absolute necessity to be realized in volume acquisition, therefore in 3D/4D, due to the variability of propagation of the electrical activity. As long as this technique is not tested and confirmed with matrix probes able to perform ultrafast imaging, these results will remain questionable from a clinical point of view.

Vascular applications

Ultrafast ultrasound imaging could also be used for the assessment of vascular stiffness using localized vessel wall pulse wave velocity and wall shear stress measurements. The conventional method of looking at vascular stiffness includes the measurement of pressure wave propagation (tonometry) over relatively long distances like carotid-brachial or carotid-femoral resulting in relative nonspecific assessment of vascular stiffness. More local assessments of different vascular beds could be important as regional vessel wall remodeling may be present and may be clinically relevant, especially in CHD. A good example is patients after coarctation of the aorta where significant differences were found in vessel wall structure proximal and distal from the coarctation[82]. Studying regional wall properties would

thus potentially add novel information. Ultrafast ultrasound allows for measurement of pulse wave velocities in shorter vessel segments. Couade et al showed using SWE that a local assessment of arterial stiffness is possible[83]. Afterwards, Maksuti et al confirmed these results comparing in vitro SWE and mechanical testing to assess arterial stiffness[84]. Concerning clinical applications, Marais el al compared local assessment (by SWE) to global assessment (by the reference technique, e.g. tonometry) in order to differentiate healthy volunteer and essential hypertensive patients. They showed that local assessment presents heterogeneous results and allows to identify the stiffest areas. Bernal et al also demonstrated that SWE could estimate the stiffness of vascular anastomoses in synthetic material[85], namely polytetrafluoroethylene (ePTFE) and polyethyleneterephthalate (Dacron). Knowing that the use of these materials is very frequent in pediatric cardiac surgery and that their stiffening is one of the most recurrent problems during the growth of children, the analysis of their stiffness seems essential. In addition, although this application seems more limited in pediatrics, the evaluation of atherosclerotic plaque by SWE is also a new tool opening new perspectives in the understanding of this disease, in particular to identify unstable plaques[86]. Ultrafast Doppler also offers the possibility to quantitatively map the vascular resistivity index over large areas as performed in the brain of neonates using trans fontanelle imaging[22]. Thanks to the very high sensitivity of ultrafast Doppler, functional brain imaging has been shown feasible in neonates by Demené et al[27].

Liver stiffness

Studying liver stiffness in cardiac patients provides information on central venous pressure (CVP) as shown almost 10 years ago[87]. Shear wave elastography has become a well-established technique for evaluating liver stiffness and has been applied to assess CVP. In a pediatric population with CHD, Jalal et al showed a strong correlation between LS and CVP

assessed during right heart catheterization[20]. Villemain et al compared LS to other parameters used in clinical practice (N-terminal pro-B-type natriuretic peptide, inferior vena cava diameter, pulsed-Doppler profile of hepatic veins) to estimate CVP (also assessed during right heart catheterization) and showed that it had the strongest correlation with CVP[19]. Moreover, LS varies over time with the CVP and could theoretically be used to monitor CVP (figure 11). This is especially important as other echographic parameters (inferior vena cava collapsibility, hepatic veins pulsed Doppler, right atrium volume) have important limitations for pediatric applications.

The importance of quantitative CVP assessment is well described for prognostication of PAH patients[88]. However, in pediatrics, due to a lack of reliable tools this parameter is not widely used to evaluate PAH. Likewise, the assessment of filling pressures in the functionally univentricular heart is limited, although important due to the preload dependence of the Fontan circulation. In addition, the significant risks of long-term hepatic impairment in patients with a functionally univentricular hearts is emerging as an increasingly important prognostic factor[89,90]. Therefore, better diagnostic tools to characterize liver morphology, stiffness and their relationship to the cardiac status and pulmonary arterial pressures in the Fontan circulation is needed. Noninvasive quantitative evaluation of right heart filling pressures was very limited before the advent of LS[21]. Therefore, quantitative assessment of CVP by SWE in this population deserves further study.

Nevertheless, the parameters that can influence liver stiffness (notably fibrosis, inflammation or cholestasis) can complicate its interpretation at the patient's bedside. As with any diagnostic tool, it should be used with an understanding of its limitations and confounding factors[21].

APPLICATION IN ADULT CARDIOLOGY – FOCUS ON CARDIAC FUNCTION AND MYOCARDIAL STIFFNESS ASSESSMENT

Since the end of the nineteenth century, the ventricular pressure-volume relation (PV loop) has become an important tool for understanding cardiovascular physiology including intrinsic ventricular pump properties, depicted by the end-systolic and end-diastolic pressure-volume relationships (ESPVR and EDPVR, respectively)[91]. By studying the volume and pressure in a cavity, assessment of hemodynamic pump parameters and of intrinsic ventricular properties became possible[92]. Likewise, strain (ε, segment length relative to a specified standardized length) can assess the contractility[93,94] and MS (μ) will impact diastolic function[95,96], especially in late diastole (EDPVR, see figure 12)[97,98].

Myocardial Compliance and EDPVR

During the passive diastolic period, myocardial stiffness reflects only the passive elastic properties of the myocardium. The EDPVR is currently the index for characterizing the passive elastic properties of the entire ventricle. Chamber stiffness is the change in ventricular pressure relative to a change in its volume (dP/dV), as reflected by the slope of the EDPVR (β). Therefore, chamber stiffness, which is by definition independent of loading conditions, is a central parameter for understanding the EDPVR and hence diastolic function. It would be useful to clinicians to be able to quantify noninvasively myocardial diastolic properties and ventricular compliance independent of the loading conditions. Current echocardiography parameters to evaluate diastolic function are dependent on loading conditions and often interdependent. Moreover, most of these parameters reflect early relaxation and not end-diastolic or passive stiffness as described by Zile et al[99]. Ultimately, clinicians need to integrate multiple parameters (including mitral inflow by pulsed wave

Doppler, mitral annular velocities by tissue Doppler imaging, pulmonary venous flow by pulsed wave Doppler, velocity of flow progression by M-mode and color Doppler) to differentiate between normal and abnormal pathological groups[100]. This particularly the case in many pathological situations, for example cardiomyopathies[101] and heart failure with reduced (HFrEF) or preserved (HFpEF) ejection fraction[102]. There is therefore a need to develop new diagnostic tools to better characterize and hence manage these patients.

During the last decade, shear wave elastography was proposed to quantify the end-diastolic myocardial stiffness. Early studies were performed and validated on large animal models such as an ovine model of infarcted myocardium[103]. Noninvasive SWI evaluation of diastolic myocardial stiffness was able to differentiate between stiff, noncompliant infarcted wall and softer wall containing stunned myocardium. This was highly correlated with local invasive measurements of the end-diastolic strain-stress relationship performed with sonomicrometers and pressure catheter[103].

Recently, several proofs of concept studies have demonstrated the possibility of estimating MS by ultrafast imaging in adults[104,50,77,52]. External acoustic radiation force was used in patients with sarcomeric hypertrophic cardiomyopathy (HCM), showing that MS was significantly higher in HCM-HFpEF patients than in healthy volunteers[77] (figure 13). Likewise, positive correlations were found between MS and echocardiographic diastolic parameters and with cardiac magnetic resonance fibrosis markers (late gadolinium enhancement, myocardial T1 pre-contrast). In addition, MS increased significantly with age in healthy volunteers, as did echocardiographic parameters used in clinical practice, as described by Caballero et al[105]. Petrescu et al, using natural valve closure, observed significantly higher MS in patients with cardiac amyloidosis compared with healthy volunteers and also increases in MS with aging[52] (figure 14). Concerning cardiac amyloidosis, Pislaru et al, working on correlation between MS and myocardial stretch,

showed a relation between patient outcome and MS estimated by this approach[51]. Investigation of MS in dilated ischemic cardiomyopathy and heart transplant were also performed, using natural valve closure[106]. Therefore, now that proof-of-concept of human application of these techniques has been demonstrated, possible applications seem numerous and varied including the assessment of diastolic function at the bedside. The challenge now is to incorporate MS into clinical management and to validate its use for the diagnosis and management of diastolic dysfunction.

Myocardial Contractility and ESPVR

During cardiac contraction, myocardial stiffness becomes driven by the myocyte contraction and matrix elasticity[107]. Therefore, myocardial stiffness must be analyzed in terms of contractile stress properties. ESPVR is a linear parameter (figure 12) and can be characterized by a slope (E_{es}, end-systolic elastance) and a volume axis intercept (V_o), so that:

$$P_{es} = E_{es}.(V_{es} - V_o) \qquad \text{Equation [2]}$$

where P_{es} and V_{es} are end-systolic pressure and volume, respectively. Importantly, this relationship was initially shown to be independent of afterload[108]. Ultimately, the ESPVR, characterizes properties of the ventricular chamber when the myocardium is at maximal activation at a given contractile state. Noninvasive measures of cardiac function are sometimes used as surrogates for systolic function. These measures include ejection fraction, wall motion, and myocardial strain. Current noninvasive measures of myocardial wall motion and function do not directly reflect myocardial contractility. MS could be a more direct parameter linked to intrinsic myocardial contractility[109,110,111]. Using PV relations, Sagawa et al[109] and Mirsky et al[112] showed the relation between myocardial stiffness and contractility. Using isolated papillary muscles, Taubert et al[110] showed that inotropic agents increase MS during systole. It has also been shown that transverse stiffness, measured using small high-

frequency indentations, is an index of contractility in beating canine interventricular septum[113]. In summary, MS could be used to better understand the systolic function.

To date, however, MS has not been used in clinical practice to measure contractility even though several studies have demonstrated that systolic MS estimated by ultrafast imaging could provide new insights into systolic function[45,114]. Pernot et al, in Langendorff perfused isolated rat hearts, demonstrated that systolic MS increased immediately after isoproterenol stimulation and followed the development of systolic pressure. They concluded that systolic MS provides a noninvasive index of myocardial contractility[45]. In the same pre-clinical model, Vejdani-Jahromi et al reached the same conclusion[114]. These experiments were performed using external acoustic radiation stimulation and ultrafast imaging in order to be able to select the timing of assessment. Nevertheless, Petrescu et al, using natural valve closure, have demonstrated that end-systole MS (just after aortic valve closure) was different between healthy volunteers and patients with cardiac amyloidosis[52]. As such, it is the only study, to date, to investigate MS for assessment of systolic function in humans. Ultrafast imaging, now applicable in clinical practice, would therefore offer the possibility of having a quantitative parameter more directly related to myocardial contractility. Nonetheless, more studies are needed to validate the clinical application of MS for assessment of systolic function.

Current clinical limitations of MS assessment by ultrafast ultrasound imaging

The main clinical limitation, common to both approaches (internal or external stimulus), is currently a segmented and not a global myocardial analysis. This is very similar to the history of speckle tracking imaging which was initially developed to allow segment analysis and then gradually improved to allow a global analysis of the heart. The stakes will be the same for the ultrafast imaging. The development of a 2D multiplane analysis or more generally a 3D

ultrafast imaging approach will probably be necessary to analyze heart as a whole. Initial pre-clinical studies are beginning to open this possibility[115,116], clinical proof-of-concept is now the next step.

Lastly, and more specifically concerning natural shear waves generated by the mitral valve, the electrical conduction through the myocardium leads to mechanical activation of myocardium too[14,37]. There are therefore two natural events that can overlap, very close in a temporal point of view. However, the sequence of myocardial activation cannot be correlated to MS, because there is no link between these two parameters. Nevertheless, it is important to be aware of electromechanical waves, which have a propagation speed in the same order of magnitude as shear waves in the myocardium, so that these events can be differentiated.

CONCLUSION

Ultrafast ultrasound imaging is a recent technology in cardiology. Because of its innovative character and the importance of the varied applications it offers, it has the potential to become a central non-invasive tool in this field. However, some questions remain unanswered and collaboration between clinicians, researchers, and manufacturers will play a key role towards achieving this goal. In this review, we aimed to shed light on current and possible future clinical applications of ultrafast ultrasound imaging in cardiology.

REFERENCES

1. Grotenhuis HB, Mertens LL. Recent evolutions in pediatric and congenital echocardiography. *Curr Opin Cardiol*. 2015;30(1):118-124. doi:10.1097/HCO.0000000000000136
2. Lai WW, Mertens LL, Cohen MS, Geva T, eds. *Echocardiography in Pediatric and Congenital Heart Disease: From Fetus to Adult, Second Edition*. Oxford, UK: John Wiley & Sons, Ltd; 2016. doi:10.1002/9781118742440
3. Forsey J, Friedberg MK, Mertens L. Speckle Tracking Echocardiography in Pediatric and Congenital Heart Disease. *Echocardiography*. 2013;30(4):447-459. doi:10.1111/echo.12131
4. Simpson J, Lopez L, Acar P, et al. Three-dimensional Echocardiography in Congenital Heart Disease: An Expert Consensus Document from the European Association of Cardiovascular Imaging and the American Society of Echocardiography. *J Am Soc Echocardiogr*. 2017;30(1):1-27. doi:10.1016/j.echo.2016.08.022
5. Cantinotti M, Kutty S, Franchi E, et al. Pediatric echocardiographic nomograms: What has been done and what still needs to be done. *Trends Cardiovasc Med*. 2017;27(5):336-349. doi:10.1016/J.TCM.2017.01.006
6. Tanter M, Fink M. Ultrafast imaging in biomedical ultrasound. *IEEE Trans Ultrason Ferroelectr Freq Control*. 2014;61(1):102-119. doi:10.1109/TUFFC.2014.6689779
7. Correia M, Provost J, Chatelin S, Villarraga HR, Tanter M, Pernot M. Ultrafast Harmonic Coherent Compound (UHCC) imaging for high frame rate echocardiography and Shear Wave Elastography. *IEEE Trans Ultrason Ferroelectr Freq Control*. 2016;63(3):420-431. doi:10.1109/TUFFC.2016.2530408
8. Villemain O, Correia M, Khraiche D, et al. Myocardial Stiffness Assessment Using

Shear Wave Imaging in Pediatric Hypertrophic Cardiomyopathy. *JACC Cardiovasc Imaging*. 2017. doi:10.1016/j.jcmg.2017.08.018

9. Song P, Bi X, Mellema DC, et al. Pediatric Cardiac Shear Wave Elastography for Quantitative Assessment of Myocardial Stiffness: A Pilot Study in Healthy Controls. *Ultrasound Med Biol*. 2016;42(8):1719-1729. doi:10.1016/J.ULTRASMEDBIO.2016.03.009
10. Maresca D, Correia M, Villemain O, et al. Noninvasive Imaging of the Coronary Vasculature Using Ultrafast Ultrasound. *JACC Cardiovasc Imaging*. 2018;11(6):798-808. doi:10.1016/j.jcmg.2017.05.021
11. Osmanski B-F, Maresca D, Messas E, Tanter M, Pernot M. Transthoracic ultrafast Doppler imaging of human left ventricular hemodynamic function. *IEEE Trans Ultrason Ferroelectr Freq Control*. 2014;61(8):1268-1275. doi:10.1109/TUFFC.2014.3033
12. de Korte CL, Nillesen MM, Saris AECM, Lopata RGP, Thijssen JM, Kapusta L. New developments in paediatric cardiac functional ultrasound imaging. *J Med Ultrason*. 2013;41(3):279-290. doi:10.1007/s10396-013-0513-9
13. Van Cauwenberge J, Lovstakken L, Fadnes S, et al. Assessing the Performance of Ultrafast Vector Flow Imaging in the Neonatal Heart via Multiphysics Modeling and In Vitro Experiments. *IEEE Trans Ultrason Ferroelectr Freq Control*. 2016;63(11):1772-1785. doi:10.1109/TUFFC.2016.2596804
14. Pernot M, Fujikura K, Fung-Kee-Fung SD, Konofagou EE. ECG-gated, Mechanical and Electromechanical Wave Imaging of Cardiovascular Tissues In Vivo. *Ultrasound Med Biol*. 2007;33(7):1075-1085. doi:10.1016/j.ultrasmedbio.2007.02.003
15. Provost J, Gambhir A, Vest J, Garan H, Konofagou EE. A clinical feasibility study of atrial and ventricular electromechanical wave imaging. *Hear Rhythm*. 2013;10(6):856-

862. doi:10.1016/j.hrthm.2013.02.028

16. Papadacci C, Finel V, Provost J, et al. Imaging the dynamics of cardiac fiber orientation in vivo using 3D Ultrasound Backscatter Tensor Imaging. *Sci Rep*. 2017;7(1). doi:10.1038/s41598-017-00946-7

17. Lee W-N, Pernot M, Couade M, et al. Mapping myocardial fiber orientation using echocardiography-based shear wave imaging. *IEEE Trans Med Imaging*. 2012;31(3):554-562. doi:10.1109/TMI.2011.2172690

18. Correia M, Deffieux T, Chatelin S, Provost J, Tanter M, Pernot M. 3D elastic tensor imaging in weakly transversely isotropic soft tissues. *Phys Med Biol*. 2018;63(15):155005. doi:10.1088/1361-6560/aacfaf

19. Villemain O, Sitefane F, Pernot M, et al. Toward Noninvasive Assessment of CVP Variations Using Real-Time and Quantitative Liver Stiffness Estimation. *JACC Cardiovasc Imaging*. 2017;10(10). doi:10.1016/j.jcmg.2017.01.018

20. Jalal Z, Iriart X, De Lédinghen V, et al. Liver stiffness measurements for evaluation of central venous pressure in congenital heart diseases. *Heart*. 2015;101(18):1499-1504. doi:10.1136/heartjnl-2014-307385

21. Pernot M, Villemain O. Stone Liver, Heart in Danger. Could the Liver Stiffness Assessment Improve the Management of Patients With Heart Failure? *JACC Cardiovasc Imaging*. 2018. doi:10.1016/j.jcmg.2017.11.024

22. Demené C, Pernot M, Biran V, et al. Ultrafast Doppler reveals the mapping of cerebral vascular resistivity in neonates. *J Cereb Blood Flow Metab*. 2014;34(6):1009-1017. doi:10.1038/jcbfm.2014.49

23. Cohen S, Liu A, Gurvitz M, et al. Exposure to Low-Dose Ionizing Radiation From Cardiac Procedures and Malignancy Risk in Adults With Congenital Heart Disease. *Circulation*. 2018;137(13):1334-1345. doi:10.1161/CIRCULATIONAHA.117.029138

24. Montaldo G, Tanter M, Bercoff J, Benech N, Fink M. Coherent plane-wave compounding for very high frame rate ultrasonography and transient elastography. *IEEE Trans Ultrason Ferroelectr Freq Control*. 2009;56(3):489-506. doi:10.1109/TUFFC.2009.1067

25. Sahn DJ. Real-time two-dimensional Doppler echocardiographic flow mapping. *Circulation*. 1985;71(5):849-853. doi:10.1161/01.CIR.71.5.849

26. Osmanski B-F, Pernot M, Montaldo G, Bel A, Messas E, Tanter M. Ultrafast Doppler imaging of blood flow dynamics in the myocardium. *IEEE Trans Med Imaging*. 2012;31(8):1661-1668. doi:10.1109/TMI.2012.2203316

27. Demené C, Deffieux T, Pernot M, et al. Spatiotemporal Clutter Filtering of Ultrafast Ultrasound Data Highly Increases Doppler and fUltrasound Sensitivity. *IEEE Trans Med Imaging*. 2015;34(11):2271-2285. doi:10.1109/TMI.2015.2428634

28. Maresca D, Correia M, Tanter M, Ghaleh B, Pernot M. Adaptive Spatiotemporal Filtering for Coronary Ultrafast Doppler Angiography. *IEEE Trans Ultrason Ferroelectr Freq Control*. 2018;65(11):2201-2204. doi:10.1109/TUFFC.2018.2870083

29. Kim HB, Hertzberg JR, Shandas R. Development and validation of echo PIV. *Exp Fluids*. 2004;36(3):455-462. doi:10.1007/s00348-003-0743-5

30. Hansen KL, Nielsen MB, Jensen JA. Vector velocity estimation of blood flow – A new application in medical ultrasound. *Ultrasound*. 2017;25(4):189-199. doi:10.1177/1742271X17713353

31. Correia M, Provost J, Tanter M, Pernot M. 4D ultrafast ultrasound flow imaging: in vivo quantification of arterial volumetric flow rate in a single heartbeat. *Phys Med Biol*. 2016;61(23):L48-L61. doi:10.1088/0031-9155/61/23/L48

32. Fadnes S, Ekroll IK, Nyrnes SA, Torp H, Lovstakken L. Robust angle-independent blood velocity estimation based on dual-angle plane wave imaging. *IEEE Trans*

Ultrason Ferroelectr Freq Control. 2015;62(10):1757-1767. doi:10.1109/TUFFC.2015.007108

33. Wigen MS, Fadnes S, Rodriguez-Molares A, et al. 4-D Intracardiac Ultrasound Vector Flow Imaging–Feasibility and Comparison to Phase-Contrast MRI. *IEEE Trans Med Imaging*. 2018;37(12):2619-2629. doi:10.1109/TMI.2018.2844552

34. Mele D, Smarrazzo V, Pedrizzetti G, et al. Intracardiac Flow Analysis: Techniques and Potential Clinical Applications. *J Am Soc Echocardiogr*. 2019;32(3):319-332. doi:10.1016/J.ECHO.2018.10.018

35. Bers DM. Cardiac excitation–contraction coupling. *Nature*. 2002;415(6868):198-205. doi:10.1038/415198a

36. Cordeiro JM, Greene L, Heilmann C, Antzelevitch D, Antzelevitch C. Transmural heterogeneity of calcium activity and mechanical function in the canine left ventricle. *Am J Physiol Heart Circ Physiol*. 2004;286(4):H1471-9. doi:10.1152/ajpheart.00748.2003

37. Provost J, Lee W-N, Fujikura K, Konofagou EE. Imaging the electromechanical activity of the heart in vivo. *Proc Natl Acad Sci U S A*. 2011;108(21):8565-8570. doi:10.1073/pnas.1011688108

38. Melki L, Grubb CS, Weber R, et al. Localization of Accessory Pathways in Pediatric Patients With Wolff-Parkinson-White Syndrome Using 3D-Rendered Electromechanical Wave Imaging. *JACC Clin Electrophysiol*. January 2019. doi:10.1016/J.JACEP.2018.12.001

39. Sandrin L, Tanter M, Catheline S, Fink M. Shear modulus imaging with 2-D transient elastography. *IEEE Trans Ultrason Ferroelectr Freq Control*. 2002;49(4):426-435. doi:10.1109/58.996560

40. Bercoff J, Tanter M, Fink M. Supersonic shear imaging: a new technique for soft

tissue elasticity mapping. *IEEE Trans Ultrason Ferroelectr Freq Control*. 2004;51(4):396-409. doi:10.1109/TUFFC.2004.1295425

41. Landau L, Liftshitz E. Theory of elasticity. *Moscow Pergamon Press*. 1965.

42. Sarvazyan AP, Rudenko O V, Swanson SD, Fowlkes JB, Emelianov SY. Shear wave elasticity imaging: a new ultrasonic technology of medical diagnostics. *Ultrasound Med Biol*. 1998;24(9):1419-1435.

43. Bercoff J, Tanter M, Fink M. Supersonic shear imaging: a new technique for soft tissue elasticity mapping. *IEEE Trans Ultrason Ferroelectr Freq Control*. 2004;51:396-409. doi:10.1109/TUFFC.2004.1295425

44. Sarvazyan AP, Rudenko O V, Swanson SD, Fowlkes JB, Emelianov SY. Shear wave elasticity imaging: a new ultrasonic technology of medical diagnostics. *Ultrasound Med Biol*. 1998;24(9):1419-1435. doi:10.1016/S0301-5629(98)00110-0

45. Pernot M, Couade M, Mateo P, Crozatier B, Fischmeister R, Tanter M. Real-time assessment of myocardial contractility using shear wave imaging. *J Am Coll Cardiol*. 2011;58(1):65-72. doi:10.1016/j.jacc.2011.02.042

46. Labeit S, Kolmerer B. Titins: Giant Proteins in Charge of Muscle Ultrastructure and Elasticity. *Science (80-).* 1995;270(5234):293-296. doi:10.1126/science.270.5234.293

47. Couade M, Pernot M, Messas E, et al. In Vivo Quantitative Mapping of Myocardial Stiffening and Transmural Anisotropy During the Cardiac Cycle. *IEEE Trans Med Imaging*. 2011;30(2):295-305. doi:10.1109/TMI.2010.2076829

48. Kanai H. Propagation of spontaneously actuated pulsive vibration in human heart wall and in vivo viscoelasticity estimation. *IEEE Trans Ultrason Ferroelectr Freq Control*. 2005;52(11):1931-1942. doi:10.1109/TUFFC.2005.1561662

49. Pislaru C, Pellikka PA, Pislaru S. Wave propagation of myocardial stretch: correlation with myocardial stiffness. *Basic Res Cardiol*. 2014;109(6):438. doi:10.1007/s00395-

014-0438-5

50. Pislaru C, Alashry MM, Thaden JJ, Pellikka PA, Enriquez-Sarano M, Pislaru S. Intrinsic Wave Propagation of Myocardial Stretch, A New Tool to Evaluate Myocardial Stiffness: A Pilot Study in Patients with Aortic Stenosis and Mitral Regurgitation. *J Am Soc Echocardiogr*. 2017;30(11):1070-1080. doi:10.1016/J.ECHO.2017.06.023

51. Pislaru C, Alashry MM, Ionescu F, et al. Increased Myocardial Stiffness Detected by Intrinsic Cardiac Elastography in Patients With Amyloidosis: Impact on Outcomes. *JACC Cardiovasc Imaging*. October 2018. doi:10.1016/J.JCMG.2018.08.014

52. Petrescu A, Santos P, Orlowska M, et al. Velocities of Naturally Occurring Myocardial Shear Waves Increase With Age and in Cardiac Amyloidosis. *JACC Cardiovasc Imaging*. February 2019. doi:10.1016/j.jcmg.2018.11.029

53. Pernot M, Villemain O. In the Heart of Stiffness: Are natural heart vibrations reliable to assess myocardial stiffness, the new Holy Grail in Echocardiography? *JACC Cardiovasc Imaging*. 2019.

54. O'Donnell M, Skovoroda AR. Prospects for elasticity reconstruction in the heart. *IEEE Trans Ultrason Ferroelectr Freq Control*. 2004;51(3):322-328. doi:10.1109/TUFFC.2004.1320788

55. Gennisson J-L, Deffieux T, Fink M, Tanter M. Ultrasound elastography: Principles and techniques. *Diagn Interv Imaging*. 2013;94(5):487-495. doi:10.1016/J.DIII.2013.01.022

56. Nash MP, Hunter PJ. Computational Mechanics of the Heart. *J Elast*. 2000;61(1/3):113-141. doi:10.1023/A:1011084330767

57. Correia M, Podetti I, Villemain O, Baranger J, Tanter M, Pernot M. Non-invasive Myocardial Shear Wave Elastography Device for Clinical Applications in Cardiology.

IRBM. 2017;38(6). doi:10.1016/j.irbm.2017.09.001

58. Caenen A, Pernot M, Peirlinck M, Mertens L, Swillens A, Segers P. An *in silico* framework to analyze the anisotropic shear wave mechanics in cardiac shear wave elastography. *Phys Med Biol*. 2018;63(7):075005. doi:10.1088/1361-6560/aaaffe

59. Papadacci C, Tanter M, Pernot M, Fink M. Ultrasound backscatter tensor imaging (BTI): analysis of the spatial coherence of ultrasonic speckle in anisotropic soft tissues. *IEEE Trans Ultrason Ferroelectr Freq Control*. 2014;61(6):986-996. doi:10.1109/TUFFC.2014.2994

60. Finel V, Papadacci C, Provost J, Tanter M, Pernot M. Motion correction for 3D ultrafast ultrasound: Application to 3D backscattered tensor Imaging of soft tissues anisotropy. In: *2017 IEEE International Ultrasonics Symposium (IUS)*. IEEE; 2017:1-1. doi:10.1109/ULTSYM.2017.8092930

61. Ramalli A, Santos P, D'hooge J. Ultrasound Imaging of Cardiac Fiber Orientation: What are We Looking at? In: *2018 IEEE International Ultrasonics Symposium (IUS)*. IEEE; 2018:1-9. doi:10.1109/ULTSYM.2018.8580100

62. Dragulescu A, Mertens L, Friedberg MK. Interpretation of Left Ventricular Diastolic Dysfunction in Children With Cardiomyopathy by EchocardiographyClinical Perspective. *Circ Cardiovasc Imaging*. 2013;6(2).

63. Friedberg MK, Mertens L. Tissue velocities, strain, and strain rate for echocardiographic assessment of ventricular function in congenital heart disease. *Eur J Echocardiogr*. 2009;10(5):585-593. doi:10.1093/ejechocard/jep045

64. Lopez L, Colan SD, Frommelt PC, et al. Recommendations for quantification methods during the performance of a pediatric echocardiogram: a report from the Pediatric Measurements Writing Group of the American Society of Echocardiography Pediatric and Congenital Heart Disease Council. *J Am Soc Echocardiogr*. 2010;23(5):465-495;

quiz 576-577. doi:10.1016/j.echo.2010.03.019

65. Song P, Bi X, Mellema DC, et al. Pediatric Cardiac Shear Wave Elastography for Quantitative Assessment of Myocardial Stiffness: A Pilot Study in Healthy Controls. *Ultrasound Med Biol*. 2016;42(8):1719-1729. doi:10.1016/j.ultrasmedbio.2016.03.009

66. Li C, Bai W, Liu Y, Tang H, Rao L. Dissipative energy loss within the left ventricle detected by vector flow mapping in diabetic patients with controlled and uncontrolled blood glucose levels. *Int J Cardiovasc Imaging*. 2017;33(8):1151-1158. doi:10.1007/s10554-017-1100-8

67. Benavidez OJ, Gauvreau K, Jenkins KJ, Geva T. Diagnostic errors in pediatric echocardiography: development of taxonomy and identification of risk factors. *Circulation*. 2008;117(23):2995-3001. doi:10.1161/CIRCULATIONAHA.107.758532

68. Fadnes S, Nyrnes SA, Torp H, Lovstakken L. Shunt Flow Evaluation in Congenital Heart Disease Based on Two-Dimensional Speckle Tracking. *Ultrasound Med Biol*. 2014;40(10):2379-2391. doi:10.1016/J.ULTRASMEDBIO.2014.03.029

69. Hansen K, Juul K, Møller-Sørensen H, Nilsson J, Jensen J, Nielsen M. Pediatric Transthoracic Cardiac Vector Flow Imaging – A Preliminary Pictorial Study. *Ultrasound Int Open*. 2019;05(01):E20-E26. doi:10.1055/a-0656-5430

70. Buck T, Mucci RA, Guerrero JL, Holmvang G, Handschumacher MD, Levine RA. The Power-Velocity Integral at the Vena Contracta. *Circulation*. 2000;102(9):1053-1061. doi:10.1161/01.CIR.102.9.1053

71. Ryan JJ, Archer SL. The Right Ventricle in Pulmonary Arterial Hypertension. *Circ Res*. 2014;115(1):176-188. doi:10.1161/CIRCRESAHA.113.301129

72. Files MD, Arya B. Pathophysiology, adaptation, and imaging of the right ventricle in Fontan circulation. *Am J Physiol Circ Physiol*. 2018;315(6):H1779-H1788. doi:10.1152/ajpheart.00336.2018

73. Friedberg MK, Redington AN. Right versus left ventricular failure: differences, similarities, and interactions. *Circulation*. 2014;129(9):1033-1044. doi:10.1161/CIRCULATIONAHA.113.001375

74. Hauser M, Bengel FM, Hager A, et al. Impaired myocardial blood flow and coronary flow reserve of the anatomical right systemic ventricle in patients with congenitally corrected transposition of the great arteries. *Heart*. 2003;89(10):1231-1235.

75. Purz S, Sabri O, Viehweger A, et al. Potential Pediatric Applications of PET/MR. *J Nucl Med*. 2014;55(Supplement 2):32S-39S. doi:10.2967/jnumed.113.129304

76. Nield LE, Dragulescu A, MacColl C, et al. Coronary artery Doppler patterns are associated with clinical outcomes post-arterial switch operation for transposition of the great arteries. *Eur Hear J - Cardiovasc Imaging*. 2018;19(4):461-468. doi:10.1093/ehjci/jex050

77. Villemain O, Correia M, Mousseaux E, et al. Myocardial Stiffness Evaluation Using Noninvasive Shear Wave Imaging in Healthy and Hypertrophic Cardiomyopathic Adults. *JACC Cardiovasc Imaging*. 2018. doi:10.1016/j.jcmg.2018.02.002

78. Maron BJ. Hypertrophic Cardiomyopathy. *JAMA*. 2002;287(10):1-18. doi:10.1001/jama.287.10.1308

79. Factor SM, Butany J, Sole MJ, Wigle ED, Williams WC, Rojkind M. Pathologic fibrosis and matrix connective tissue in the subaortic myocardium of patients with hypertrophic cardiomyopathy. *J Am Coll Cardiol*. 1991;17(6):1343-1351. doi:10.1016/S0735-1097(10)80145-7

80. Delgado-Olguín P. Embryological Origins: How Does the Right Ventricle Form. In: *Right Ventricular Physiology, Adaptation and Failure in Congenital and Acquired Heart Disease*. Cham: Springer International Publishing; 2018:1-17. doi:10.1007/978-3-319-67096-6_1

81. Friedberg MK, Redington AN. Right ventricular physiology, adaptation and failure in congenital and acquired heart disease. *Book, Springer Int Publ*. 2018.

82. Sarkola T, Redington AN, Slorach C, Hui W, Bradley T, Jaeggi E. Assessment of vascular phenotype using a novel very-high-resolution ultrasound technique in adolescents after aortic coarctation repair and/or stent implantation: relationship to central haemodynamics and left ventricular mass. *Heart*. 2011;97(21):1788-1793. doi:10.1136/hrt.2011.226241

83. Couade M, Pernot M, Prada C, et al. Quantitative assessment of arterial wall biomechanical properties using shear wave imaging. *Ultrasound Med Biol*. 2010;36(10):1662-1676. doi:10.1016/j.ultrasmedbio.2010.07.004

84. Maksuti E, Widman E, Larsson D, Urban MW, Larsson M, Bjällmark A. Arterial Stiffness Estimation by Shear Wave Elastography: Validation in Phantoms with Mechanical Testing. *Ultrasound Med Biol*. 2016;42(1):308-321. doi:10.1016/J.ULTRASMEDBIO.2015.08.012

85. Bernal M, Sen I, Urban MW. Evaluation of materials used for vascular anastomoses using shear wave elastography. *Phys Med Biol*. 2019;64(7):075001. doi:10.1088/1361-6560/ab055c

86. Ramnarine K V, Garrard JW, Kanber B, Nduwayo S, Hartshorne TC, Robinson TG. Shear wave elastography imaging of carotid plaques: feasible, reproducible and of clinical potential. *Cardiovasc Ultrasound*. 2014;12(1):49. doi:10.1186/1476-7120-12-49

87. Millonig G, Friedrich S, Adolf S, et al. Liver stiffness is directly influenced by central venous pressure. *J Hepatol*. 2010;52(2):206-210. doi:10.1016/j.jhep.2009.11.018

88. Galiè N, Humbert M, Vachiery J-L, et al. 2015 ESC/ERS Guidelines for the diagnosis and treatment of pulmonary hypertension. *Eur Heart J*. 2016;37(1):67-119.

doi:10.1093/eurheartj/ehv317

89. Lui G, Saidi A, Bhatt AB, et al. Diagnosis and Management of Noncardiac Complications in Adults With Congenital Heart Disease: A Scientific Statement From the American Heart Association. *Circulation*. 2017;136(20). doi:10.1161/CIR.0000000000000535

90. Daniels CJ, Bradley EA, Landzberg MJ, et al. Fontan-Associated Liver Disease. *J Am Coll Cardiol*. 2017;70(25):3173-3194. doi:10.1016/j.jacc.2017.10.045

91. Suga H, Sagawa K. Instantaneous pressure-volume relationships and their ratio in the excised, supported canine left ventricle. *Circ Res*. 1974;35(1):117-126.

92. Burkhoff D, Mirsky I, Suga H. Assessment of systolic and diastolic ventricular properties via pressure-volume analysis: a guide for clinical, translational, and basic researchers. *Am J Physiol Heart Circ Physiol*. 2005;289(2):H501-12. doi:10.1152/ajpheart.00138.2005

93. Greenberg NL, Firstenberg MS, Castro PL, et al. Doppler-derived myocardial systolic strain rate is a strong index of left ventricular contractility. *Circulation*. 2002;105(1):99-105.

94. Abraham TP, Nishimura RA. Myocardial strain: can we finally measure contractility? *J Am Coll Cardiol*. 2001;37(3):731-734.

95. Zile MR, Brutsaert DL. New concepts in diastolic dysfunction and diastolic heart failure: Part I: diagnosis, prognosis, and measurements of diastolic function. *Circulation*. 2002;105(11):1387-1393.

96. Borbély A, van der Velden J, Papp Z, et al. Cardiomyocyte Stiffness in Diastolic Heart Failure. *Circulation*. 2005;111(6):774-781. doi:10.1161/01.CIR.0000155257.33485.6D

97. Mirsky I, Pasternac A, Ellison RC. General index for the assessment of cardiac

function. *Am J Cardiol*. 1972;30(5):483-491. doi:10.1016/0002-9149(72)90038-0

98. Fester A, Samet P. Passive elasticity of the human left ventricle. The parallel elastic element. *Circulation*. 1974;50(3):609-618.

99. Zile MR, Baicu CF, Gaasch WH. Diastolic heart failure--abnormalities in active relaxation and passive stiffness of the left ventricle. *N Engl J Med*. 2004;350(19):1953-1959. doi:10.1056/NEJMoa032566

100. Nagueh SF, Smiseth OA, Appleton CP, et al. *Recommendations for the Evaluation of Left Ventricular Diastolic Function by Echocardiography: An Update from the American Society of Echocardiography and the European Association of Cardiovascular Imaging*. Vol 29.; 2016. doi:10.1016/j.echo.2016.01.011

101. Elliott PM, Anastasakis A, Borger MA, et al. 2014 ESC Guidelines on diagnosis and management of hypertrophic cardiomyopathy. *Eur Heart J*. 2014.

102. Yancy CW, Jessup M, Bozkurt B, et al. 2017 ACC/AHA/HFSA Focused Update of the 2013 ACCF/AHA Guideline for the Management of Heart Failure. *J Am Coll Cardiol*. 2017;70(6):776-803. doi:10.1016/j.jacc.2017.04.025

103. Pernot M, Lee W-N, Bel A, et al. Shear Wave Imaging of Passive Diastolic Myocardial Stiffness: Stunned Versus Infarcted Myocardium. *JACC Cardiovasc Imaging*. 2016;9(9):1023-1030. doi:10.1016/j.jcmg.2016.01.022

104. Song P, Bi X, Mellema DC, et al. Quantitative Assessment of Left Ventricular Diastolic Stiffness Using Cardiac Shear Wave Elastography. *J Ultrasound Med*. 2016;35(7):1419-1427. doi:10.7863/ultra.15.08053

105. Caballero L, Kou S, Dulgheru R, et al. Echocardiographic reference ranges for normal cardiac Doppler data: results from the NORRE Study. *Eur Hear J - Cardiovasc Imaging*. 2015.

106. Strachinaru M, Bosch JG, van Dalen BM, et al. Cardiac Shear Wave Elastography

Using a Clinical Ultrasound System. *Ultrasound Med Biol*. 2017;43(8):1596-1606. doi:10.1016/j.ultrasmedbio.2017.04.012

107. McCain ML, Yuan H, Pasqualini FS, Campbell PH, Parker KK. Matrix elasticity regulates the optimal cardiac myocyte shape for contractility. *Am J Physiol Circ Physiol*. 2014;306(11):H1525-H1539. doi:10.1152/ajpheart.00799.2013

108. Suga H, Sagawa K, Shoukas AA. Load independence of the instantaneous pressure-volume ratio of the canine left ventricle and effects of epinephrine and heart rate on the ratio. *Circ Res*. 1973;32(3):314-322.

109. Sagawa K, Suga H, Shoukas AA, Bakalar KM. End-systolic pressure/volume ratio: a new index of ventricular contractility. *Am J Cardiol*. 1977;40(5):748-753. doi:10.1016/0002-9149(77)90192-8

110. Taubert K, Willerson JT, Shapiro W, Templeton GH. Contraction and resting stiffness of isolated cardiac muscle: effects of inotropic agents. *Am J Physiol*. 1977;232(3):H275-82. doi:10.1152/ajpheart.1977.232.3.H275

111. Royse CF, Royse AG, Rohrlach R, Wright CE, Angus JA. The cardiovascular effects of adrenaline, dobutamine and milrinone in rabbits using pressure-volume loops and guinea pig isolated atrial tissue. *Anaesth Intensive Care*. 2007;35(2):180-188.

112. Mirsky I, Tajimi T, Peterson KL. The development of the entire end-systolic pressure-volume and ejection fraction-afterload relations: a new concept of systolic myocardial stiffness. *Circulation*. 1987;76(2):343-356.

113. Livingston JZ, Halperin HR, Yin FCP. Accounting for the Gregg effect in tetanised coronary arterial pressure-flow relationships. *Cardiovasc Res*. 1994;28(2):228-234. doi:10.1093/cvr/28.2.228

114. Vejdani-Jahromi M, Freedman J, Nagle M, Kim Y-J, Trahey GE, Wolf PD. Quantifying Myocardial Contractility Changes Using Ultrasound-Based Shear Wave

Elastography. *J Am Soc Echocardiogr*. 2017;30(1):90-96. doi:10.1016/J.ECHO.2016.10.004

115. Gennisson J, Provost J, Deffieux T, et al. 4-D ultrafast shear-wave imaging. *IEEE Trans Ultrason Ferroelectr Freq Control*. 2015;62(6):1059-1065. doi:10.1109/TUFFC.2014.006936

116. Papadacci C, Bunting EA, Wan EY, Nauleau P, Konofagou EE. 3D Myocardial Elastography In Vivo. *IEEE Trans Med Imaging*. 2017;36(2):618-627. doi:10.1109/TMI.2016.2623636

FIGURES

Figure 1: Conventional and ultrafast ultrasound imaging
On the left, conventional imaging with focused emission. On the right, ultrafast imaging with plane wave emission.

Figure 2: Stiffness assessment by external stimulus
The shear wave is initiated by an external stimulus and then visualized by ultrafast imaging. On B-Mode acquisition, we can see the propagation of the shear wave and deduced the shear wave speed (Vc). [courtesy from Villemain et al, ref[77]]

Figure 3: Stiffness assessment by internal stimulus
Here, the shear wave is generated by an internal stimulus (valve closure) and the ultrafast imaging allows to see its propagation. On M-Mode acquisition along the midline of the LV septum, a spatiotemporal representation of the local tissue acceleration is obtained and allows to estimate the shear wave speed (Vc) [courtesy from Petrescu et al, ref[52]]

Figure 4: Different technological approaches (internal or external stimulus) to assess myocardial stiffness using ultrafast ultrasound imaging
The natural shear waves have a very variable propagation directivity and a wavelength that could make their analysis subject to bias. On the other hand, the shear wave generated by acoustic radiation force requires a more local analysis.

Figure 5 : Pediatric myocardial stiffness assessment by Shear Wave Elastography
(A) Elastography results. (B) Fractional anisotropy results. [courtesy of Villemain et al[8], with authorization of Elsevier]
HCM = hypertrophic cardiomyopathy; HV = healthy volunteer.

Figure 6: Shunts assessment. Comparison between conventional color flow imaging (CFI) and vector flow imaging by speckle tracking (ST)
VSD shunt (on the left) and ASD shunt (on the right) assessed by vector flow imaging.
LA = left atrium; LV = left ventricle; LVOT = left ventricle outflow tract; RA = right atrium; RV = right ventricle
[courtesy of Fadnes et al[68], with authorization of Elsevier]

Figure 7: 4D vector flow imaging
3D rendering of the flow path lines in three parts of the cardiac cycle corresponding to diastole, diastasis and systole, respectively.
[courtesy of Wigen et al[33], with authorization of IEEE]

Figure 8: Coronary Ultrafast Doppler Angiography (CUDA). Intramural coronary vasculature in open-chest swine.
Sub-epicardial arterioles are successfully detected using ultrafast Doppler imaging. Upper panels show a long axis view of venous coronaries in mid-systole (left) and arterial coronaries in mid-diastole (right). Lower panels show a mid-level short axis view of venous coronaries in mid-systole (left) and arterial coronaries in mid-diastole (right). [courtesy of Maresca et al[10], with authorization of Elsevier]

Figure 9: Myocardial fiber orientation assessed by Backscatter Tensor Imaging (BTI)

3D representation of fibers orientation in the left ventricle of an open-chest sheep at four different moments of the cardiac cycle
[courtesy of Papadacci et al[16] and Nature Journals; No change has been made. http://creativecommons.org/licenses/by/4.0/.]

Figure 10: Electromechanical wave imaging on patients before and after successful radiofrequency ablation of accessory pathways
Figure published by Melki et al (ref 10). Thanks to EWI, the authors were able to compare noninvasively electrical activation delays, before (A) and after (B) radiofrequency ablation of accessory pathways. [courtesy of Melki et al[38], with authorization of Elsevier]

Figure 11: Correlation between liver stiffness and central venous pressure (CVP), pre- and post-volume loading, with an example of evaluation of liver stiffness by shear wave elastography (kPa).
Correlation between liver stiffness and central venous pressure (CVP), pre- and post-volume loading, with an example of evaluation of liver stiffness by shear wave elastography (kPa). [courtesy of Villemain et al[19], with authorization of Elsevier]

Figure 12: Pressure-Volume relations
Left: the 4 phases of the cardiac cycle are readily displayed on the PV loop, which is constructed by plotting instantaneous pressure vs. volume. This loop repeats with each cardiac cycle and shows how the heart transitions from its end-diastolic state to the end-systolic state and back. Right: with a constant contractile state and afterload resistance, a progressive reduction in ventricular filling pressure causes the loops to shift toward lower volumes at both end systole and end diastole. When the resulting end-systolic PV points are connected, a reasonably linear end-systolic PV relationship (ESPVR) is obtained. The linear ESPVR is characterized by a slope (Ees) and a volume axis intercept (Vo). In contrast, the diastolic PV points define a nonlinear end diastolic PV relationship (EDPVR). [courtesy from Burkhoff et al, adapted from ref[92]]

Figure 13: Myocardial Stiffness in adult hypertrophic cardiomyopathy (HCM) and healthy volunteer (HV)
Comparison of MS between HCM group (in red) and HV group (in green). [courtesy of Villemain et al[77], with authorization of Elsevier]

Figure 14: Variation of shear wave velocity at mitral valve closure with the degree of diastolic function and E/E' in adult population (healthy volunteer and cardiac amyloidosis)
A) Shear wave velocities are shown after the mitral valve closure increase with the severity of diastolic dysfunction (grades: 0 to 3) (B) Correlation between shear wave propagation velocity after mitral valve closure and conventional echocardiographic parameter of diastolic function, E/E'. Correlation line have been fitted only to data points corresponding to cardiac amyloidosis patients. (Pink) Healthy volunteers; (green) cardiac amyloidosis.
[courtesy from Petrescu et al, ref[52]]

Central Illustration. Ultrafast Imaging in Cardiology
Possible applications of ultrafast ultrasound imaging in cardiology

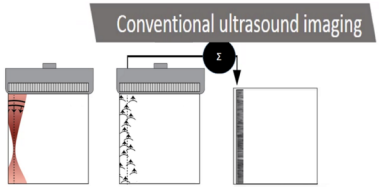

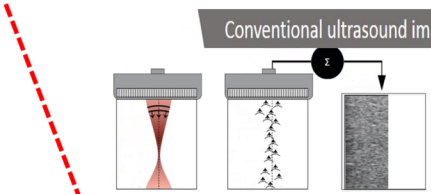

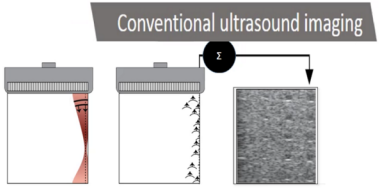

≈ 25 to 50 frames / second

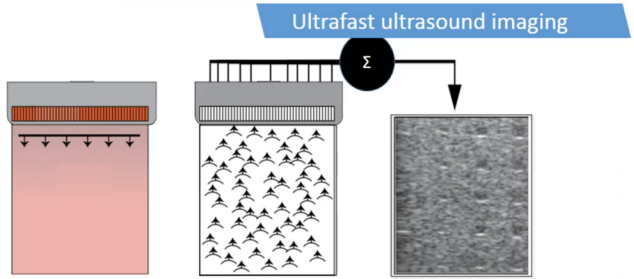

≈ 2500 to 5000 frames / second

External Stimulus and UF imaging

Step 1: External Stimulus by Acoustic Radiation Force

Step 2: UF imaging

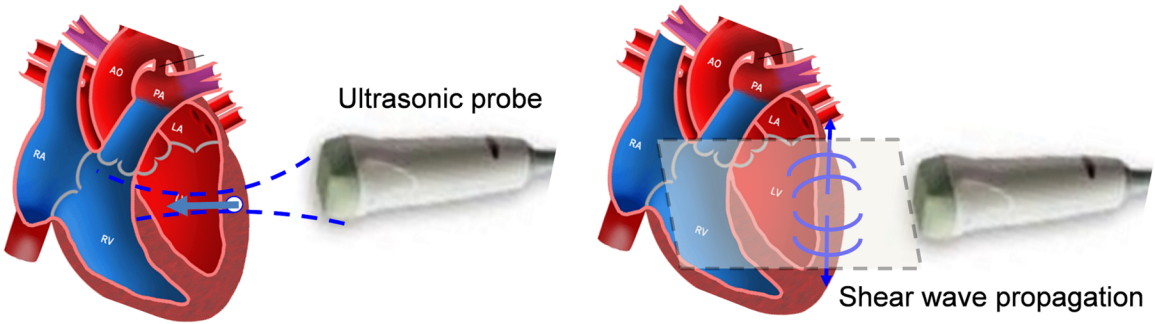

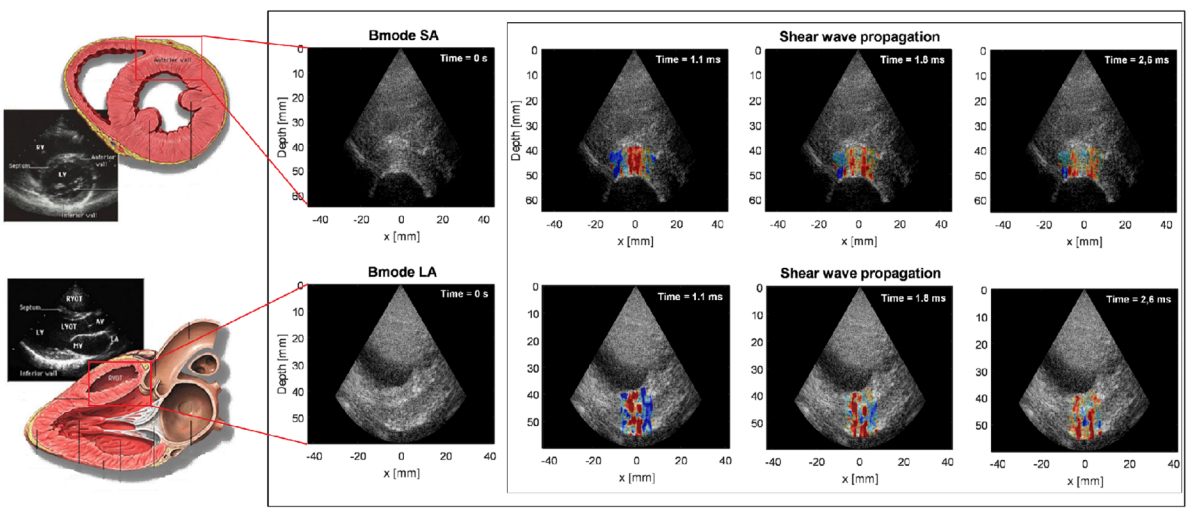

Internal Stimulus and UF imaging

Step 1: Internal Stimulus by Valve closures

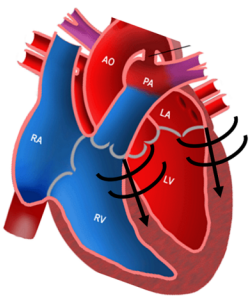

Begetting of natural shear wave

Step 2: UF imaging

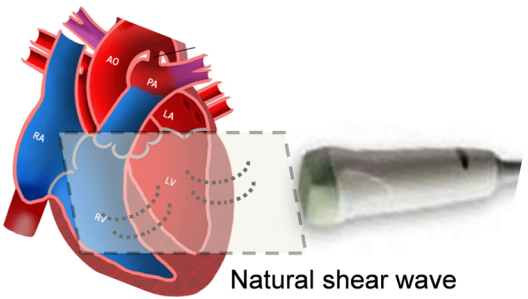

Natural shear wave propagation

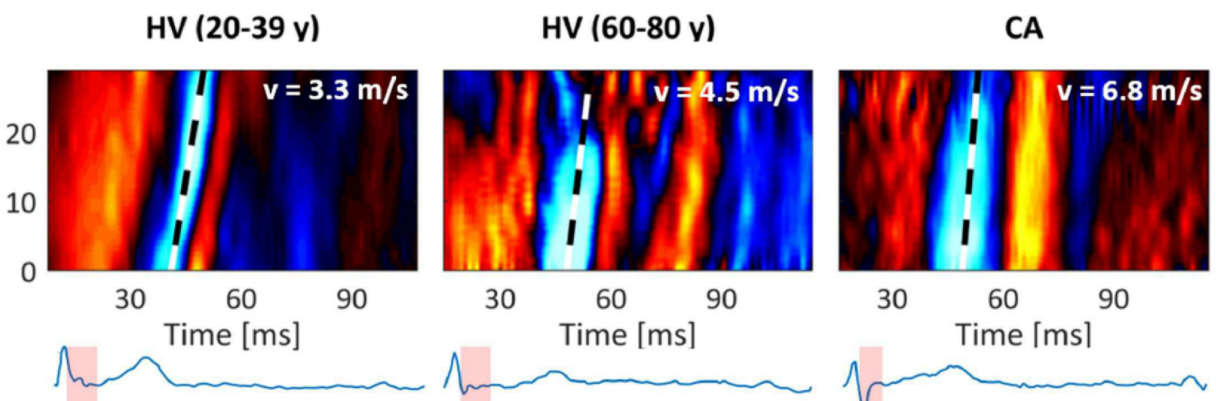

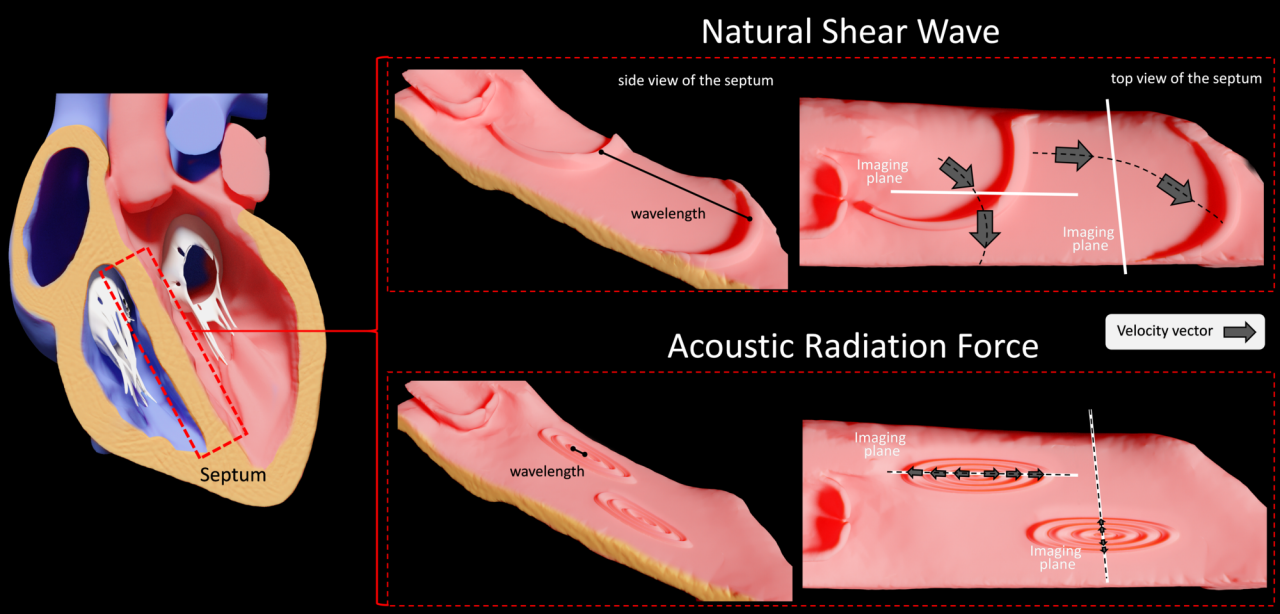
Natural Shear Wave
side view of the septum
top view of the septum
wavelength
Imaging plane
Imaging plane
Velocity vector
Acoustic Radiation Force
wavelength
Imaging plane
Imaging plane
Septum

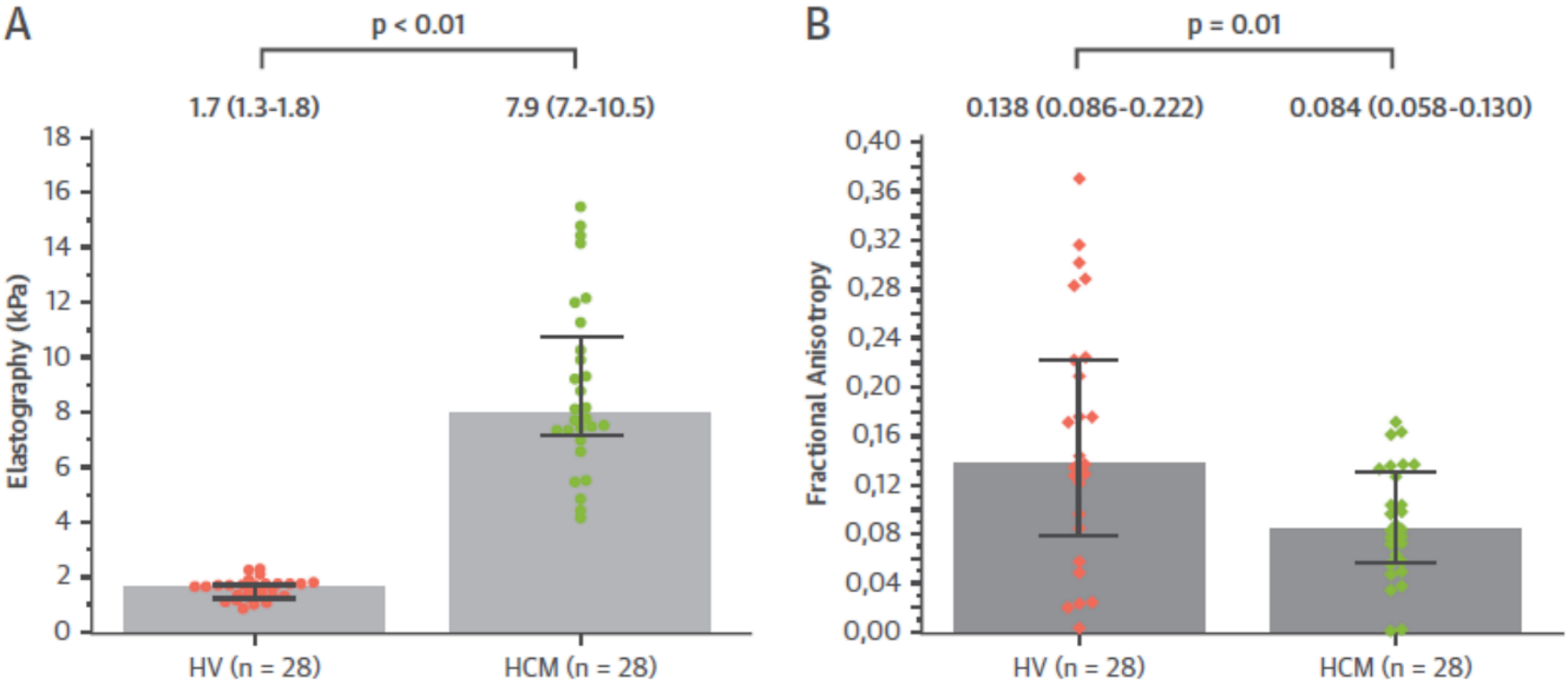
A
p < 0.01
1.7 (1.3-1.8)
7.9 (7.2-10.5)
Elastography (kPa)
18
16
14
12
10
8
6
4
2
0
HV (n = 28)
HCM (n = 28)
B
p = 0.01
0.138 (0.086-0.222)
0.084 (0.058-0.130)
Fractional Anisotropy
0,40
0,36
0,32
0,28
0,24
0,20
0,16
0,12
0,08
0,04
0,00
HV (n = 28)
HCM (n = 28)

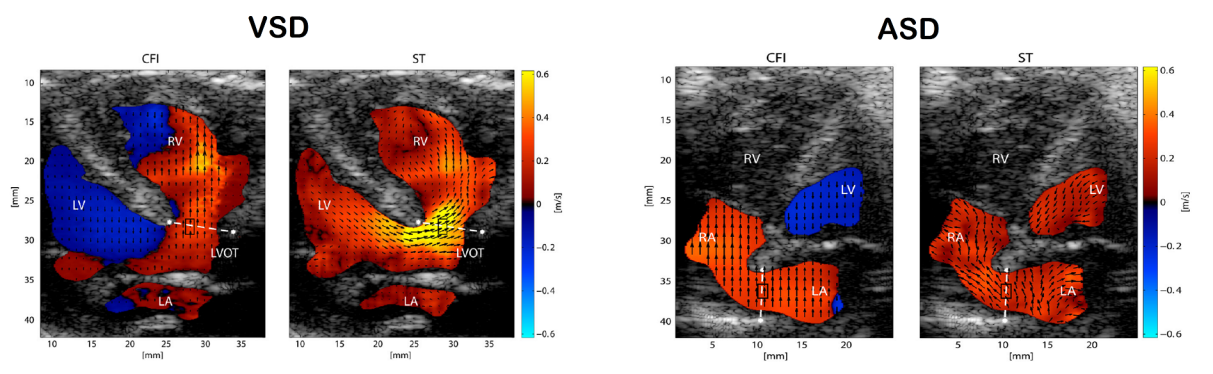
VSD
CFI
ST
RV
LV
LVOT
LA
[mm]
[m/s]
0.6
0.4
0.2
0
−0.2
−0.4
−0.6
ASD
CFI
ST
RV
LV
RA
LA
[mm]
[m/s]

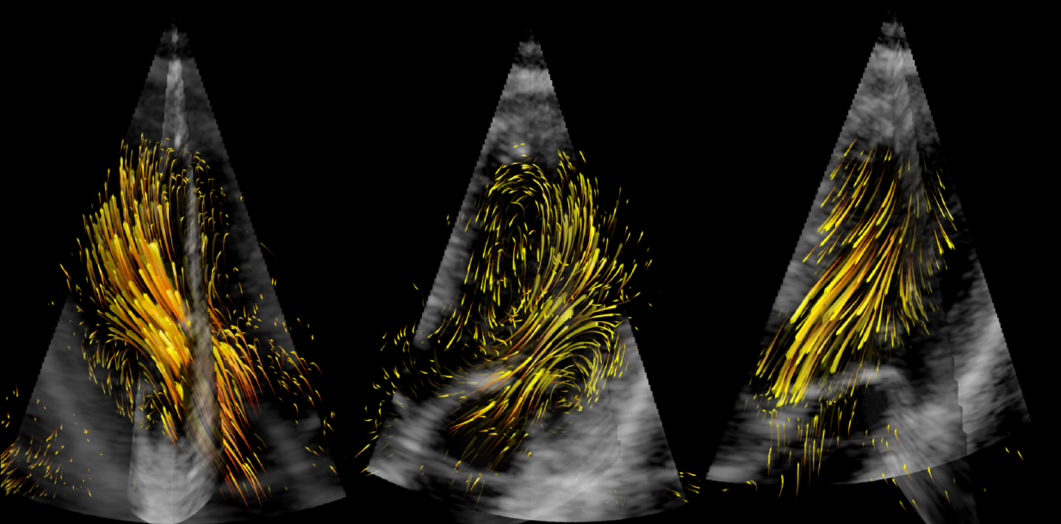

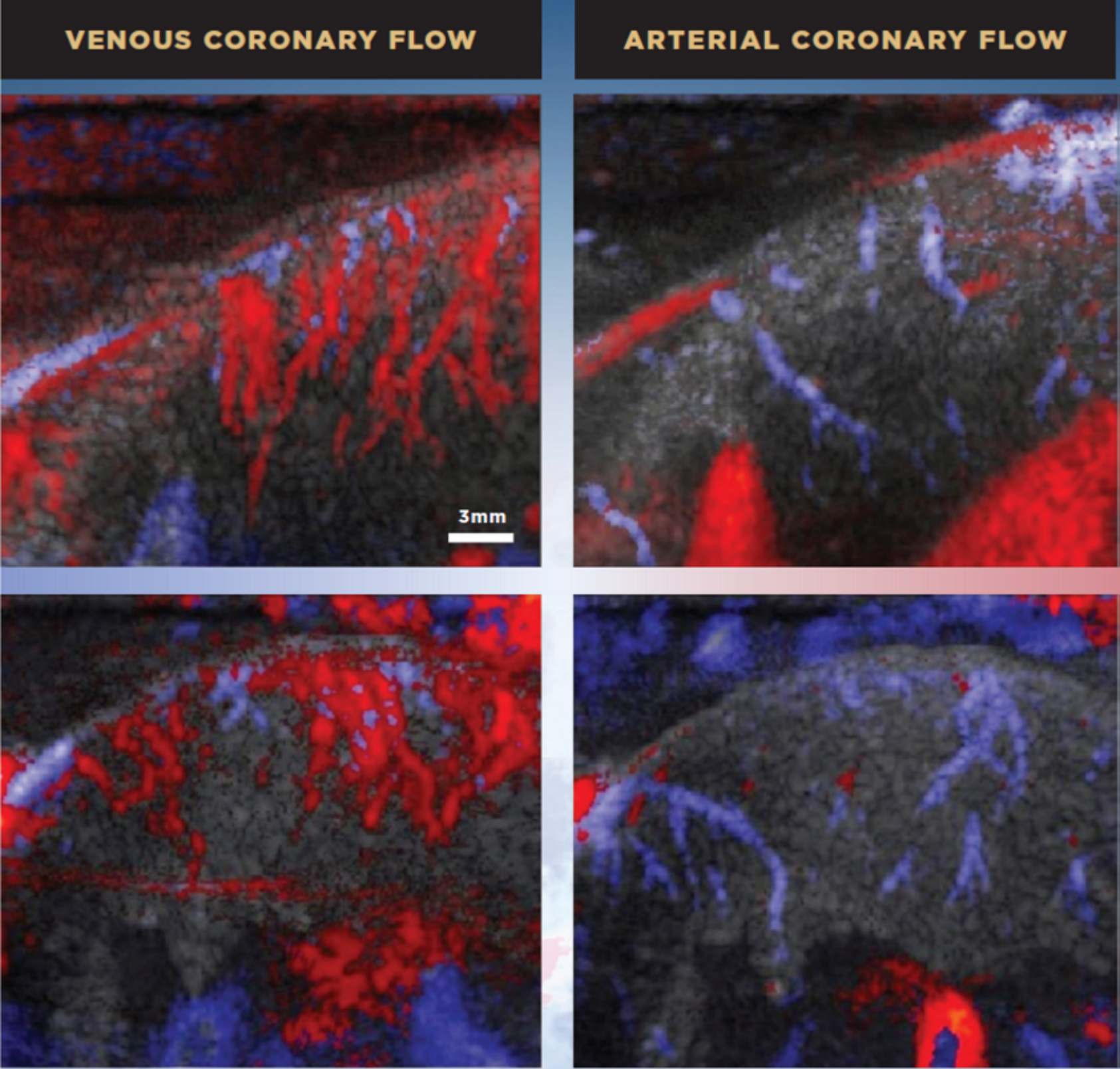
VENOUS CORONARY FLOW
ARTERIAL CORONARY FLOW
3mm

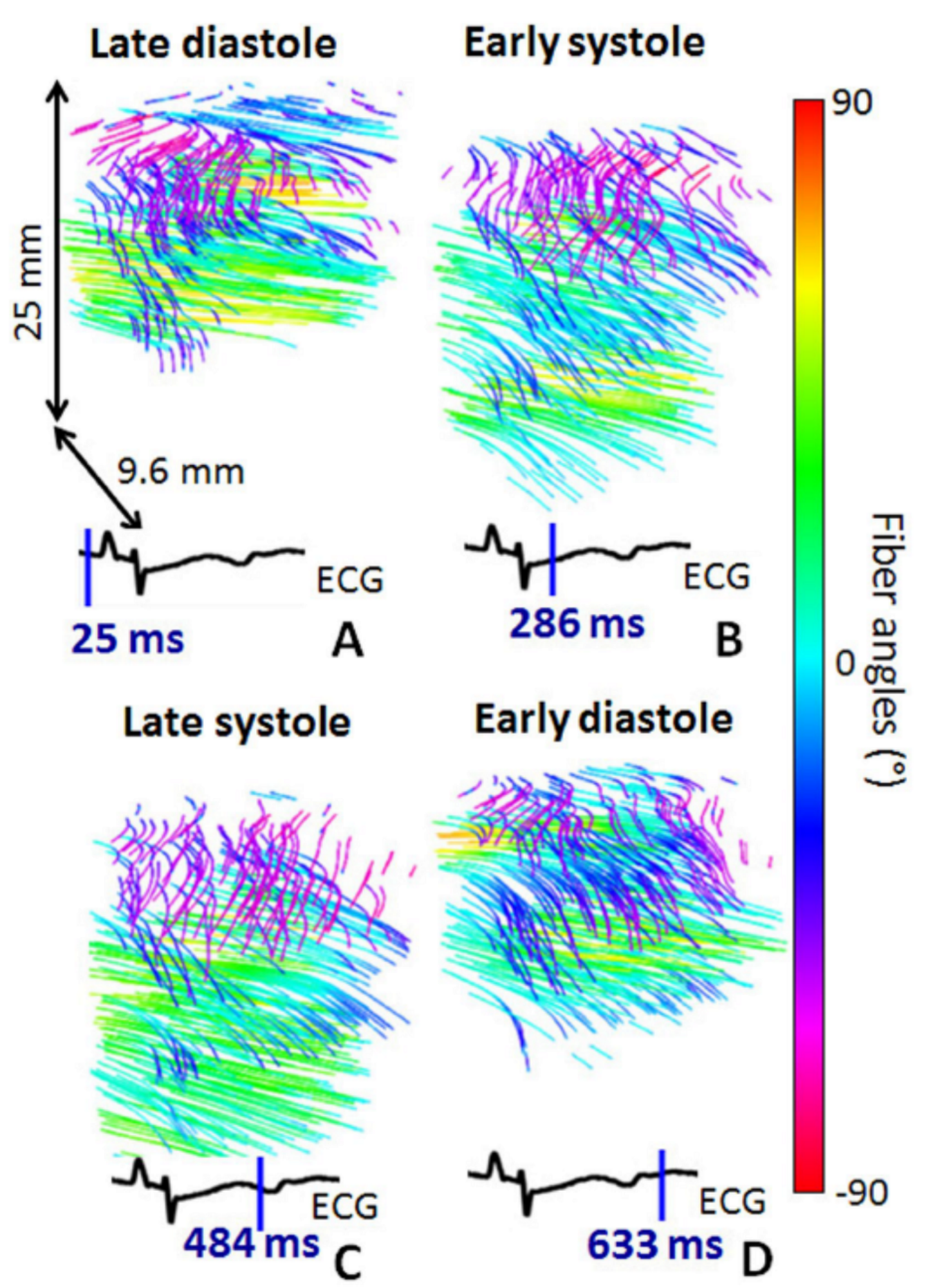
Late diastole
Early systole
25 mm
9.6 mm
ECG
25 ms
A
ECG
286 ms
B
Late systole
Early diastole
ECG
484 ms
C
ECG
633 ms
D
90
0
-90
Fiber angles (°)

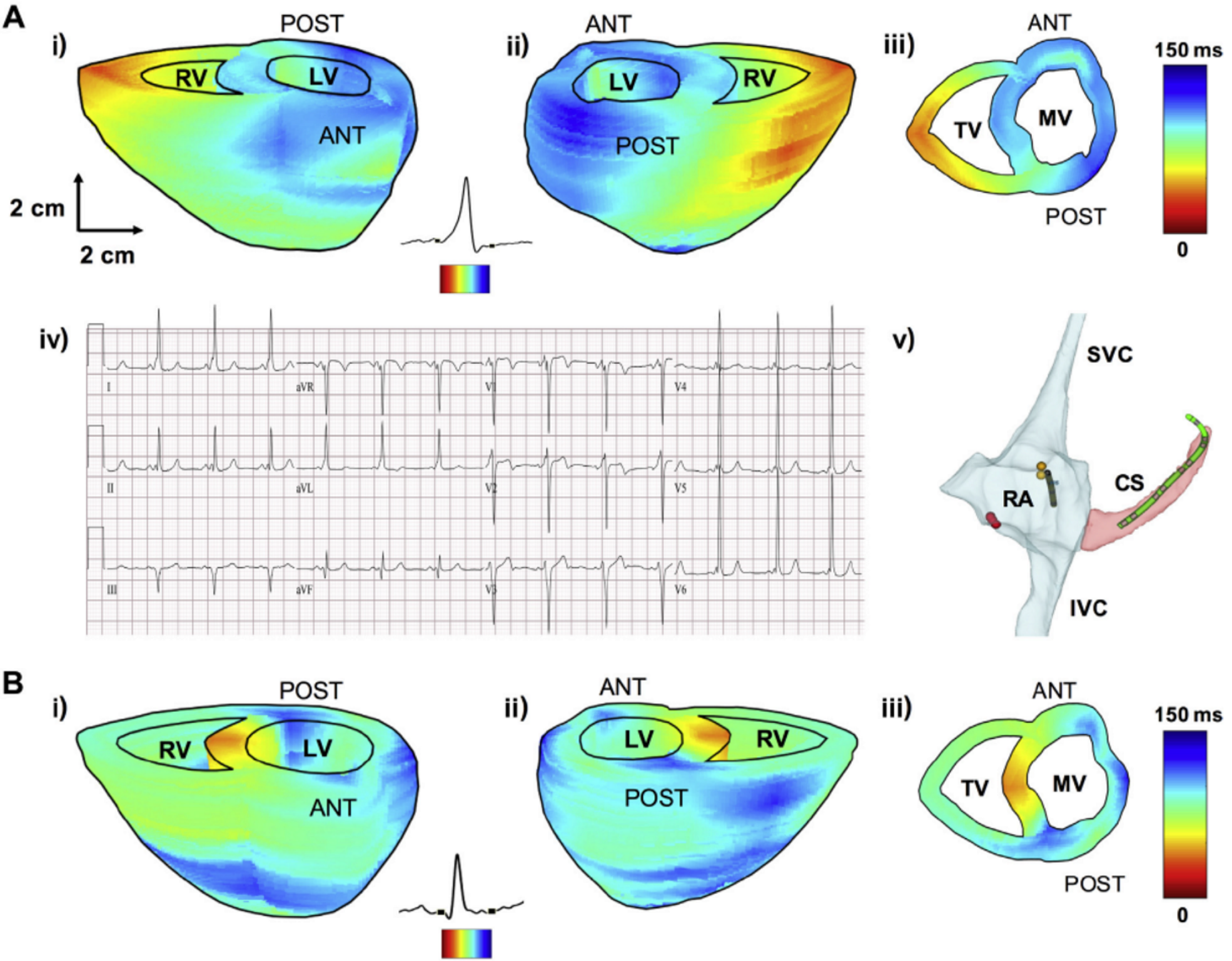
A
i)
POST
RV
LV
ANT
2 cm
2 cm
ii)
ANT
LV
RV
POST
iii)
ANT
TV
MV
POST
150 ms
0
iv)
I
aVR
V1
V4
II
aVL
V2
V5
III
aVF
V3
V6
v)
SVC
RA
CS
IVC
B
i)
POST
RV
LV
ANT
ii)
ANT
LV
RV
POST
iii)
ANT
TV
MV
POST
150 ms
0

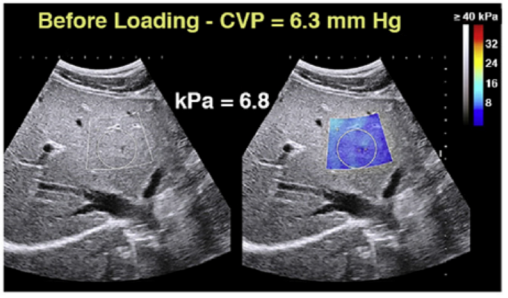
Before Loading - CVP = 6.3 mm Hg
kPa = 6.8
≥ 40 kPa
32
24
16
8

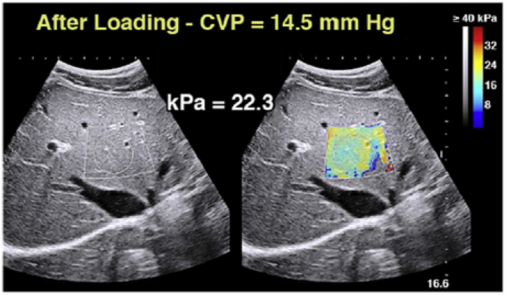
After Loading - CVP = 14.5 mm Hg
kPa = 22.3
≥ 40 kPa
32
24
16
8
16.6

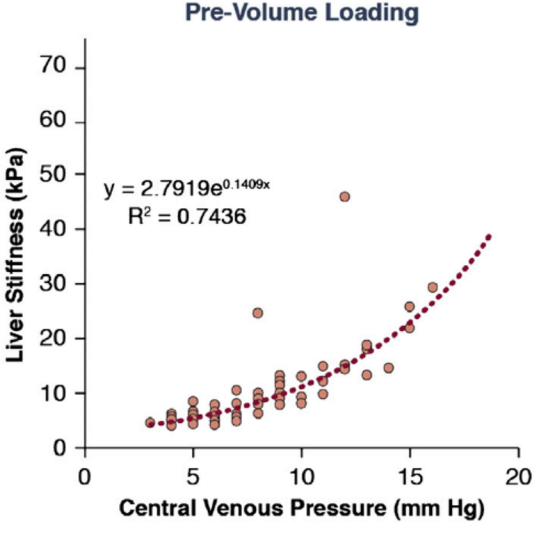
Pre-Volume Loading
y = 2.7919e^0.1409x
R² = 0.7436
Liver Stiffness (kPa)
Central Venous Pressure (mm Hg)
0
10
20
30
40
50
60
70
0
5
10
15
20

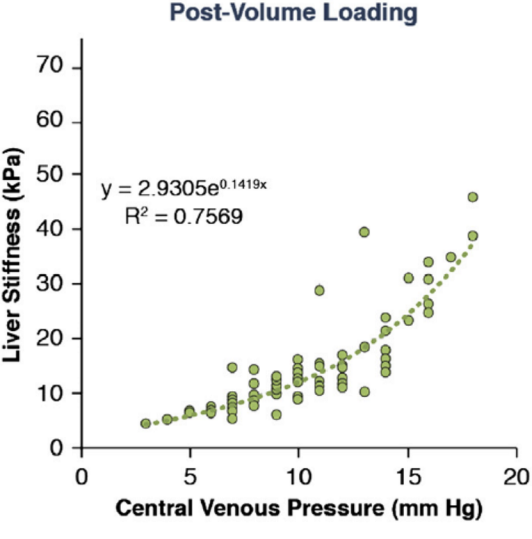
Post-Volume Loading
y = 2.9305e^0.1419x
R² = 0.7569
Liver Stiffness (kPa)
Central Venous Pressure (mm Hg)
0
10
20
30
40
50
60
70
0
5
10
15
20

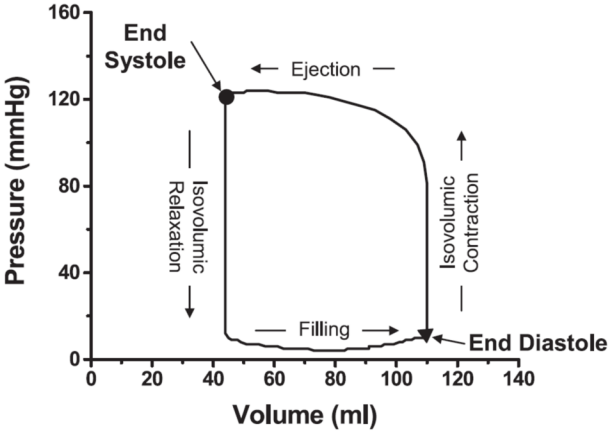
160
120
80
40
0
Pressure (mmHg)
0
20
40
60
80
100
120
140
Volume (ml)
End
Systole
Ejection
Isovolumic
Relaxation
Isovolumic
Contraction
Filling
End Diastole

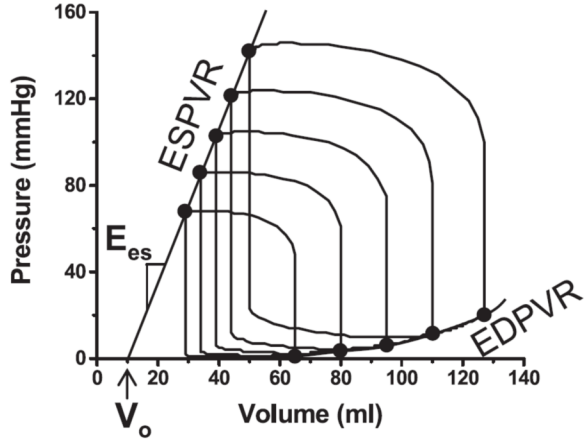
160
120
80
40
0
Pressure (mmHg)
0
20
40
60
80
100
120
140
Volume (ml)
ESPVR
EDPVR
E
es
V
o

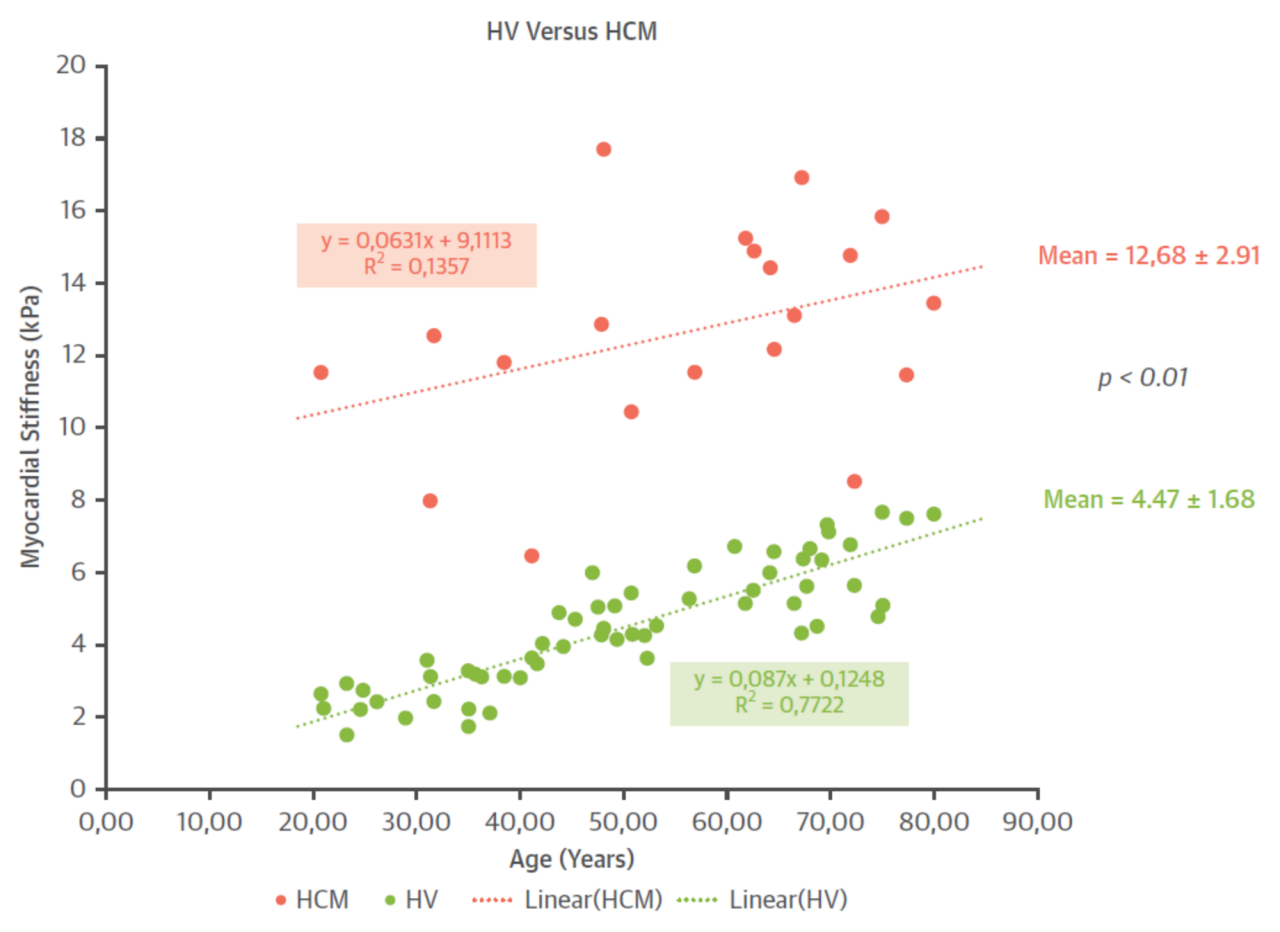
HV Versus HCM
Myocardial Stiffness (kPa)
Age (Years)
y = 0,0631x + 9,1113
R2 = 0,1357
Mean = 12,68 ± 2.91
p < 0.01
Mean = 4.47 ± 1.68
y = 0,087x + 0,1248
R2 = 0,7722
HCM
HV
Linear(HCM)
Linear(HV)

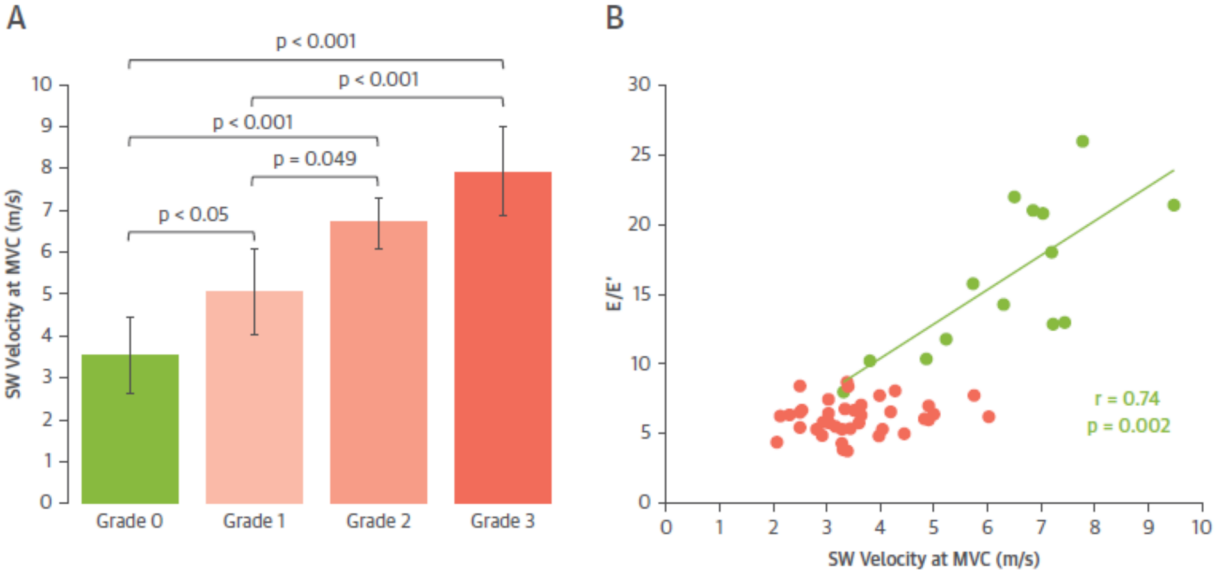
A
p < 0.001
p < 0.001
p < 0.001
p = 0.049
p < 0.05
SW Velocity at MVC (m/s)
0
1
2
3
4
5
6
7
8
9
10
Grade 0
Grade 1
Grade 2
Grade 3
B
E/E'
0
5
10
15
20
25
30
0
1
2
3
4
5
6
7
8
9
10
SW Velocity at MVC (m/s)
r = 0.74
p = 0.002